ASTRONOMY & ASTROPHYSICS
SUPPLEMENT SERIES

Astron. Astrophys. Suppl. Ser. **108,** 669-694 (1994)

Low resolution IUE spectra of Wolf-Rayet stars*,**

A. Niedzielski and K. Rochowicz

Institute of Astronomy N. Copernicus University, ul. Chopina 12/18, 87-100 Toruń, Poland

Received August 16, 1993; accepted June 4 ,1994

Abstract. — We present uniformly reduced and measured equivalent widths, FWHM and observed line fluxes for 94 "single" WR stars (34 galactic WN, 22 galactic WC, 31 LMC WN and 7 LMC WC) based on the archive IUE spectra of WR stars gathered from different observational runs and from different epochs. The spectra are used for spectral classification in the ultraviolet region and for searching correlations among the strength and widths of emission lines of different ions. Some correlations with optical and near IR lines observed by other authors are given as well. The set of spectra we use is almost complete to 12 magnitude and representative according to spectral subtype of WR stars.

Key words: atlases — stars: classification — stars: Wolf-Rayet

1. Introduction

Since their discovery in 1867 (Wolf & Rayet 1867) Wolf-Rayet (WR) stars have been intensively studied by both observers and theoreticians. The most characteristic feature of these stars-their dense, opaque and fast moving envelopes-make interpretation of their spectra very difficult. Therefore, details concerning their physics are still not very precise. Neither the strong emission lines in their spectra nor the shape of their continua can be analyzed by standard methods established during many years of research of more or less "standard" stars. The observed high reddenings to many of these very distant stars farther inhibits their analysis. Altogether these circumstances result in uncertainty of such fundamental stellar parameters as luminosities, temperatures, masses, intrinsic colors and chemical composition.

At present it is commonly accepted that WR stars are end points of evolution of the most massive stars. There is, however, another approach to these objects, according to which, they are considered even the pre-main sequence objects (Underhill 1991). This disaccordance in interpretation of WR spectra illustrates well the scale of problems connected with understanding of WR stars.

Without deciding what WR stars are one can subdivide them into three sequences, according to appearance of strong emission lines in their optical spectra: WN and WC (Beals & Plaskett 1935) with dominating nitrogen and carbon lines, respectively, and WO (Barlow & Hummer 1982) as most extreme WC stars with very strong oxygen lines. In this paper we will not deal with Population II WR stars, the so-called [WR] stars, met frequently in the Planetary Nebulae Nuclei. All these three sequences can be further subdivided into WN2, WN3, ... WN9, WC4, WC5, ... WC9 and WO1, WO2, ... WO4 subtypes according to the relative strength of various optical lines of helium (HeI, HeII), nitrogen (NIII, NIV, NV), carbon (CII, CIII, CIV) and oxygen (OIII, OIV, OV, OVI) - Smith (1968). By analogy to MK classification WR subtypes are frequently divided into early (WNE, WCE) and late (WNL, WCL) subtypes, but this is not strictly connected to any stellar parameter. The spectral classification of WR stars is purely phenomenological and cannot not be interpreted as a sequence of effective temperatures in any case.

The strange content of WR spectra (lack or weakness of hydrogen lines, strong CNO element lines) suggests peculiar chemical composition of their envelopes. This proved to be real and now we are quite sure that WR stars envelopes are mostly composed of helium, with nitrogen being much overabundant in WN envelopes. In the case of WC stars carbon is the next after helium most abundant element. Hydrogen is absent or much underabundant in all WR stars (see Nugis 1991 for a review of chemical composition).

For the most recent review of WR stars properties the reader is referred to van der Hucht (1992).

Many extensive observational programs were devoted to mass analysis of optical and IR spectra of WR stars (Vreux et al. 1983; Conti et al. 1983; Torres & Conti 1984; Torres 1985; Torres et al. 1986; Conti & Massey 1989; Conti et al. 1989; Conti et al. 1990; Vreux et al. 1990) but the ultraviolet line spectra of these stars were considered

*Based on archive IUE spectra from Vilspa

**Table 6 is only available electronically at the CDS via anonymous ftp. 130.79.128.5

only for some of them (Nussbaumer et al. 1982; Smith & Willis 1983; Willis et al. 1986).

The aim of the current paper is to give a detailed description of UV spectra of as many galactic and LMC WR stars as possible. For that purpose we present uniformly measured equivalent widths (EW), full widths at half maximum (FWHM) and observed line fluxes for all measurable from low resolution IUE spectra emission lines in the program 94 stars. The spectral classification of WR stars in UV is discussed on the basis of both shape of the spectra and correlations of line equivalent widths and line widths with spectral subtype. We also discuss emission line correlations between different lines of many ions.

2. Observational material and reduction

Ultraviolet observations of WR stars, prior to IUE, have generally been restricted to either broad-band photometric or low resolution spectrophotometric measurements and a review of such material is given by Willis (1980). With the advent of the IUE satellite a large number of WR stars, both in the Galaxy and the Magellanic Clouds, have become accessible to detailed UV observations, covering the wavelength range $\lambda\lambda$ 1150–3250. The satellite, its scientific instrument and performance have been described by Boggess et al. (1978a,b). As part of the numerous programmes investigating the UV spectra of WR stars, many objects have been observed, both with the satellite's low resolution ($\sim$ 6 Å) and high resolution ($\sim 0.1 - 0.2$ Å) spectroscopic modes. Each star was observed usually utilizing both short-wavelength (SWP camera: $\lambda\lambda$ 1150–2000) and long-wavelength (LWR or LWP camera: $\lambda\lambda$ 1850–3250) spectrographs. In addition, for each wavelength range, large aperture (LAP: 10" × 20") or small aperture (SAP: 3" × 3") – or both – spectra were recorded.

The ultraviolet spectra of the WR stars used in this study were obtained from Vilspa IUE archive. We have tried to select as many single and SB1 type stars as possible in the Galaxy and the LMC to get the complete, flux-calibrated spectra between 1150 and 3250 Å. Altogether 56 stars in the Galaxy (listed in Table 1) and 38 in the LMC Table 2) (note that this is about one third of the number of known galactic and LMC WR stars, see Table 3 where the number of stars in our sample to all known so far is compared) were found, for which at least single SWP and LWR (or LWP) low resolution images are accessible.

The WNE/L and WCE/L spectral subtypes were attributed to all stars from Table 1 according to Conti & Massey (1989).

We have requested two images for each wavelength range when available. The stars and associated IUE images used in this analysis are listed in Table 4.

Initially, all the spectra were reduced to standard MELO extracted spectral files, including corrections for wavelength scales and relative intensities. However, to avoid the problems with different intensity transfer functions (ITF), they were recorded as flux numbers (FN) and then transformed into the form of absolute energy fluxes using the calibrations given by Bohlin & Holm (1980).

Table 1. The program galactic WR stars (monochromatic v magnitudes from Massey (1984) or Torres & Massey (1988). In parentheses there are given v magnitudes from Van der hucht et al. (1988), * - the b magnitude is given instead of v; colon denotes an uncertain value

WR	Identification	Sp Type	v
1	4004	WN 5	10.54
2	6327	WN 2	11.33
3	9974	WN 3+a(SB)	10.70
4	16523	WC 5	10.75
5	17638	WC 6	11.17
6	50896	WN 5(SB1)	7.3
7	56925	WN 4	11.79
10	65865	WN 4.5	11.1
12	CD-45 4482	WN 7(SB1)	11.05
14	76536	WC 6	9.6
15	79573	WC 6	11.85
16	86161	WN 8	8.52
17	88500	WC 5	11.18
18	89358	WN 5	11.19
22	92740	WN 7+a(SB1	7.20
23	92809	WC 6	9.91
24	93131	WN 7+a	7.3
25	93162	WN 7+a	8.87
33	95435	WC 5	12.63
40	96548	WN 8	7.7
44	LSS 2289	WN 4	(12.96)
50	LSS 3013	WC 6+a	12.5
52	115473	WC 5	10.13
53	117297	WC 8	11.20
55	117688	WN 7	(10.87)
56	LS 8	WC 7	14.23
57	119078	WC 7	10.30
61	LSS 3208	WN 4.5	12.46
69	136488	WC 9	(9.43)
71	143414	WN 6(SB1)	10.30
75	147419	WN 6	11.27
78	151932	WN 7	(6.61)
85	LSS 3982	WN 6	10.7
86	156327	WC 7	9.72
90	156385	WC 7	(7.45)
92	157451	WC 9	10.65
103	164270	WC 9(SB1?)	9.18
104	Ve2-45	WC 9	(13.54)
106	E313643	WC 9	12.65
108	E313846	WN 9	10.16
110	165688	WN 6	10.26
111	165763	WC 5	8.41
123	177230	WN 8(SB1)	11.27
128	187282	WN 4(SB1)	10.56
134	191765	WN 6(SB1)	8.24
135	192103	WC 8	8.50
136	192163	WN 6(SB1)	7.64
138	193077	WN 6+a(SB1)	8.11
141	193928	WN 6(SB1)	10.14
148	197406	WN 7(SB1)	10.46
152	211564	WN 3	11.69
154	213049	WC 6	11.69
155	214419	WN 7(SB1)	8.74
156	AC+60 38562	WN 8	11.10
157	219460	WN 4.5	9.93
158	AS 513	WN 7	11.46

The reduction procedures and the measurements were performed using the software facilities (ReWiA v2.0) of the Institute of Astronomy in Toruń (Borkowski 1992). We have decided to rebin all the images into linear wavelength with constant dispersion step of 2.5 Å. Intensity points which are saturated or fall outside the range of

Table 2. The program LMC WR stars (see Table 1 for notes)

Br	Identification	Sp Type	v
1	L-10, FD1	WN 3	16.04
3	WS 1, FD2	WN 3	14.91
6	32109	WN 3p	13.91
7	32125	WC 5	15.18
8	32257	WC 5-6	15.12
10	32402	WC 5	14.01
12	268847	WN 3	14.73
13	33133	WN 8	12.81
14	269015	WN 4	14.52
15	L-115,FD14	WN 4	14.86
18	269227	WN 9-10	12.09
19	34783	WN 3	14.96
23	AL-140,FD22	WN 3	14.71
24	AL-150,FD23	WN 7	13.35
25	AB-16	WN 3	15.62
26	36063	WN 7	12.70
27	WS20, FD25	WN 3	14.93
29	269485	WN 3/WCE	14.73
35	269549	WN 4	14.95
38	AB-2	WN 3	15.53
40	269624	WN 3	14.99
43	37026	WC 5	14.16*
46	269692	WN 3	14.80
50	37680	WC 5	14.27
56	FD51	WN 5:	13.76
58	AB-4	WN 5-6	15.54
59	AL-348,FD52	WN 3	
62	269818	WC 5	14.0:
64	W27/23,FD56	WN 9-10	13.30
71	269883	WN 7	
80	R135, FD64	WN 7	13.07
89	38282	WN 7	11.20
90	269928	WN 7	12.06
92	38344	WN 6	13.03
93	FD73	WC 6-7	16.5
98	AL-412,FD78	WN 4	
99	AL-414,FD79	WN 4	14.99
100	270149	WN 3-4	14.66

the ITF curves employed were omitted. The SAP spectra complement the LAP data and sometimes cover regions in the latter spectra which suffer from saturation effects. However, because the SAP transmission is less then 100%, this aperture spectra are relative. In order to convert the SAP data to absolute fluxes we have determined an appropriate conversion factor (from the empirical ratio of the LAP and SAP data) in each case. This procedure was already applied by Nussbaumer et al. (1982). When available, two or more spectra for each wavelength range were averaged. Finally, for each star, the short-wavelength and long-wavelength spectra were spliced at a common wavelength (overlapping fragments being averaged).

Continuum was fitted using splines to by-eye selected line free points from the spectra after careful estimation of its shape for different spectral subclasses. This procedure is obviously a subjective one and may result in systematic errors of EW and FWHM. The equivalent widths, FWHM and line fluxes (F_λ) were measured either by fitting Gaussian profiles to the emission lines (or separate Gaussians to the blends) using FIT or through profile integration with the AREA procedures of ReWiA. The estimated accuracy of the measurement of the line strengths in earlier studies was usually of the order of 0.1 in the log of the EW (e.g. Conti et al. 1983; Torres et al. 1986). An intercomparison of independent measures of separate spectra of several stars gave us a formal σ of ± 0.06. We have also plotted the number of lines measured repeatedly as the function of the value of error (in %) – see Fig. 1.

The comparison of our results with those of Nussbaumer et al. (1982) for galactic and Smith & Willis (1983) for LMC stars gives us an estimate of our systematic errors connected with the EW determination. We can estimate the difference of measured values in this and previous papers by averaging for all commonly measured lines, the ratio of the difference in numerical values of EW to the mean of these two numbers, which give us the mean value of maximum error. We can also calculate the appropriate correlation coefficient (r). For the former paper we obtained the maximum error of 22% (0.09 dex) and r=0.99 while for the latter the maximum error of 28% (0.12 dex) and r=0.98. See also Figs. 2a and 2b, where we compare our values with those mentioned above.

Taking into account the "internal" (the same lines measured several times) and "external" (comparison with other authors) errors we believe that our equivalent widths and line fluxes are accurate to some 20–30%. Basing on "internal" error estimation only, we assume that with the values of FWHM a 10–15% error is connected.

3. Line identification

Nussbaumer et al. (1982) have already discussed general spectral characteristics of WR stars ultraviolet spectra. They proposed an identification scheme considering only the main contributor for each emission line. This simple scheme was usually adopted in subsequent papers dealing with IUE low resolution spectra. The problem was emphasized and considered more thoroughly only in some papers devoted to high resolution spectra of WR stars (Willis et al. 1986; Koenigsberger 1990). We found it relevant to examine once more the identification of all accessible emission lines for both WN and WC subclasses. Given many possibilities for line identifications in ultraviolet range, we restricted our search to the following species: HeI, HeII, NIII, NIV, NV, OIII, OIV, OV, OVI, CII, CIII, CIV, SiIII, SiIV. However, some other species appearing in blends are mentioned occasionally in the following subsections. See Table 5 where a selection of the strongest UV lines for ions listed above basing on Striganow & Odincowa (1982) is given. To construct a list of the most likely set of contributors to a given line we took into account the abundance of the element, the degree of ionization and transition probability. The discussion is given below.

3.1. *WN stars*

Altogether up to 18 emission lines were measured in the spectra of WN stars (Table 6); we propose the following

identification for them, starting from the shortest wavelength:

λ1241 Å due to NV transition $2s^2S-2p^2P^0$ with two unresolved components; usually strong; weaker or even very weak in late subclasses;
λ1284 Å – unblended, but unconspicuous result of NIV $3d^1D-4p^1P^0$ transition;
λ1310 Å with broader profile, which suggests a contribution to NIV $3p^1P^0-3p'^1P$ from SiIII;
λ1375 Å attributed to FeV, PIII, SiIII ions by Koenigsberger (1990) not far from expected OV $2p^1P^0-2p^2\ ^1D$;
λ1406 Å SiIV $3s^2S-3p^2P^0$ emission with possible OV-OVI contribution;
λ1486 Å strong and present throughout the WN sequence, clearly the outcome of NIV $2s^2\ ^1S-2p^3P^0$;
λ1551 Å very strong and well known from strong P-Cygni absorption carbon resonance doublet CIV $2s^2S-2p^2P^0$ with possible insignificant NV contribution;
λ1620 Å a series of NV transitions clearly blended with neighboring HeII emission peak;
λ1640 Å the strongest line for the bulk of WN stars; the effect of HeII $2p^2P^0-3d^2D$ (counterpart of Balmer-α) transition;
λ1720 Å quite broad feature predominated by NIV $2p^1P^0-2p^2\ ^1D$ or/and NIII ions; the contribution from SiIV should be noticed, mainly for later subtypes;
λ1750 Å complex transition of NIII, mainly $2p^2\ ^2P-2p3\ 2D^0$;
λ2215 Å the shortest wavelength for HeII Fowler $(n-3)$ series line (11-3) $3d^2D-11f^2F^0$, revealing weekly only in exceptional cases;
λ2253 Å the next HeII line of this series (10-3) $3d^2D-10f^2F^0$, distinctly marked in several spectra, blended with NIII;
λ2306 Å the successive (9-3) $3d^2D-9f^2F^0$ HeII feature, found still only for individual stars; blend with SiIII;
λ2385 Å the following (8-3) $3d^2D-8f^2F^0$ HeII line, possibly blended with OIII and OIV;
λ2511 Å "the show goes on"... (7-3) $3d^2D-7f^2F^0$ line, the first one of this series clearly visible and measured for the majority of WN stars; possible contribution from OIV and SiIV;
λ2733 Å (6-3) $3d^2D-6f^2F^0$ HeII transition, usually strong enough to exhibit the pronounced profile, probably not affected by blending;
λ2984 Å due mainly to NIII $3p'^2P-3d'^2P^0$ as its strength increase towards later subclasses, however the contribution from NV should be important in WNE;
λ3203 Å HeII (5-3) $3d^2D-5f^2F^0$ line, in most cases sufficiently suffering from detector noise (proximity of long wavelength scope) to neglect the contributors... (like OIV, SiIII – if any).

3.2. *WC stars.*

Up to 28 lines in IUE low resolution spectra of WC stars were measured (Table 6). Here is an identification for them:

λ1176 Å the first evidence of carbon presence: CIII $2p^3P^0-2p^2\ ^3P$ triplet appreciable at the short wavelength limit;
λ1215 Å Lyman-α (with probably insignificant HeII $2p^2P^0-4d^2D$ contribution) with its great variety of the strength;
λ1247 Å carbon once more: CIII $2p^1P^0-2p^2\ ^1S$ transition;
λ1307 Å two blended components of SiIII: $3p^3P^0-3p^2\ ^3P$ and $3p^1P^0-4s^1S$;
λ1343 Å the strongest OIV $2p^2\ ^2P-2p^3\ ^2D^0$ transition, generally blended with CII $2p^2P^0-2p^2\ ^2D$ resonance lines;
λ1375 Å a fairly strong emission behaving as might be expected for OV $2p^1P^0-2p^2\ ^1D$;
λ1406 Å OIV $2p^2P^0-2p^2\ ^4P$ intercombination lines blended with the resonance lines of SiIV $3s^2S-3p^2P^0$;
λ1551 Å the resonance doublet of CIV $2s^2S-2p^2P^0$; fully developed P-Cygni absorption profile;
λ1620 Å CIII $3p^3P^0-4d^3D$ transition clearly blended with neighboring HeII emission;
λ1640 Å the effect of HeII $2p^2P^0-3d^2D$ (counterpart of Balmer-α) transition, substantial contribution comes from CIV (Hillier 1989; Hamann et al. 1992) and CIII λ 1645 (Hamann et al. 1992);
λ1725 Å mainly due to SiIV $3d^2D-4p^2P^0$, although NIV may be present as a blend (Willis 1980);
λ1815 Å unidentified – Willis et al. (1986) suggest SiII here;
λ1909 Å CIII $2s^2\ ^1S-2p^3P^0$ intercombination line blended with 1923 CIII 4 f^3F-3d^3D (Hamann et al. 1992);
λ2297 Å strong CIII $2p^1P^0-2p^2\ ^1D$ emission together with SiIII and HeII (9-3) $3d^2D-9f^2F^0$;
λ2330 Å two carbon competitors: CIV $5g^2G-8h^2H^0$ and CII $2p^2P^0-2p^2\ ^4P$;
λ2385 Å (8-3) $3d^2D-8f^2F^0$ HeII line, possibly blended with OIII and OIV;
λ2405 Å two carbon competitors again: CIV $4p^2P^0-5d^2D$ and CII $2p^2P^0-5s^2S$;
λ2511 Å (7-3) $3d^2D-7f^2F^0$ HeII blended with CII and less so SiIV and OIV, the red wing of the profile often strongly distorted or wholly incepted by the following emission;
λ2530 Å CIV complex – three transitions ($4d^2D-5f^2F^0$, $4f^2F^0-5g^2G$, $4f^2F^0-5f^2F^0$) forming a broad structure; together with the previous λ2511 Å blend as well as with SiIII emission which follows;
λ2595 Å CIV $4d^2D-5p^2P^0$ doublet with a contribution from OIII, CIII peak at the red wing is usually noticed;

λ2699 Å two carbon doublets: CIII $4p^3P^0-6s^3S$ and CIV $4p^2P^0-5s^2S$ feeded by OV;
λ2733 Å (6-3) $3d^2D-6f^2F^0$ HeII slightly affected by CIII $4f^3F^0-6g^3G$;
λ2787 Å OV $3s^3S-3p^3P^0$ triplet in the middle of similar structure of CIII $4f^1F^0-6g^1G$;
λ2837 Å CII $2p^2\ ^2S-3p^2P^0$ transition with OIV contributor;
λ2906 Å CIV $5g^2G-7h^2H^0$ emission, again OIV probably contributes;
λ3070 Å two oxygen competitors: OIV $3s^2S-3p^2P^0$ and possibly OVI $6s^2S-7p^2P^0$;
λ3130 Å complex broad emission of oxygen, different ions to be involved, e.g. OIII, OVI $7g^2G-9h^2H^0$ and OV $3p^1P^0-3d^1D$;
λ3203 Å (5-3) $3d^2D-5f^2F^0$ HeII line, again at the edge of detected spectrum, thus likely contribution of OIV and SiIII is difficult to confirm.

4. Emission line strengths

The gathered spectra cover all subtypes of WR stars and allow us to follow the line spectrum changes with spectral type. Representative tracings for every WN subtype are shown in Figs. 3a and 3b, while for majority of WC subtypes in Fig. 4. The broad depression in the middle of the tracings is, of course, the result of interstellar reddening – famous, 2200 Å "bump". We would try to get rid of it in a subsequent paper. We ignore also here the influence of ferrum quasi-continuum (Nugis & Sapar 1985) as well, although it may influence the determined line equivalent widths and FWHM through the uncertainity in continuum fixing for shorter wavelengths.

The equivalent widths, FWHM, and observed (reddened) fluxes are given in Table 6. Let us remind here that whenever we say "equivalent width" we mean equivalent width of an emission component. Even when an emission line is connected with a P Cygni absorption, we did not measure the absorption component, neither we accounted for it in EW of emission.

4.1. *WN stars*

In Figs. 3a and 3b we see a montage of UV spectra of early (WNE) and late (WNL) nitrogen sequence stars, respectively. One can easily notice changes in ionization state in WN envelopes as going form WN 2 to WN 9. Among the strongest emission lines NIII, NIV and NV as well as HeII and CIV may be examined.

Two close, strongest lines namely CIV λ 1551 and HeII λ 1640 seem to behave in a similar way, although EW data for HeII λ 1640 are more scattered. Their intensity increases from WN 2 to WN 4-5. In latter subtypes they disappear gradually and in WN 9 are very weak, or not seen at all. Similar behavior present NIV λ 1486 and SiIV λ 1406. The equivalent widths for these two lines seem to increase for WNE and decrease for WNL, their maximum intensity seems to be reached in WN 4-5.

Nitrogen NV λ 1241 line, as seen in Fig. 3, seems to decrease its intensity (EW) from WN2 to WN 9 systematically, while NIII λ 1750 increases continuously from earliest to latest WN subtypes. NIII λ 1750 is very weak or not seen in WN 2 and WN 3 stars. It becomes noticeable in WN 4, WN 4.5. Then its intensity grows, and in WN 7 it is clearly seen while in WN 8 it becomes as strong as NIV λ 1720 or even stronger in WN 9. An important, easy noticeable, identification of spectral type is then NIII λ 1750 to NIV λ 1720 ratio. It is not blend-free, unfortunately.

The behavior of various UV lines of different ions is also presented in Figs. 5, 6 and 7, where some relations between equivalent widths and spectral subtype are given. These figures confirm our description of spectral effects in UV region, they show, however, that the scatter of equivalent widths for stars of a given subtype is large, as it was already concluded on the basis of optical spectra by Conti et al. (1983). This scatter is most evident in Figs. 5 and 6. In Fig. 5a-e we can see a relation of emission lines equivalent width with spectral subtype for NIII, NIV, NV, CIV and SiIV respectively. One can easily notice the large scatter mentioned above. Even when the overall relation is clearly seen, as it is in the case of NIII - Fig. 5a correlation is weak (correlation coefficient r=0.55). Figure 6a,b presents the emission lines of two strongest UV HeII lines plotted vs. spectral subtype. As it is seen in Fig 6a. no straight correlation exists for HeII λ 1640. The second strong HeII line - λ 3203 seems to be correlated with spectral type rather weakly or not at all – Fig. 6b.

We studied also line ratios versus spectral subtype relations (see Fig. 7a-c). Only NIII to NV ratio (here NIII λ 1750 to NV λ 1241 is shown) seems to correlate relatively well (r=0.76) for WN stars. However, a trend of higher ionization toward earlier subtypes is observed in each case.

Studying precisely Figs. 5 and 6, one can notice that the LMC WN stars of WN3 and WN 4 subtypes have stronger HeII, NV, NIV, NIII, CIV lines than their galactic counterparts. One could conclude, that this is a selection effect since LMC WNE stars in our sample are more numerous than galactic. In case of WN 7, however, the selection effect is not so strong since LMC stars are almost as numerous as galactic, this effect is also noticeable in HeII λ 1640 (Fig. 6a).

4.2. *WC stars*

The ultraviolet spectra of WC stars are much more complicated (as it is in optical and NIR) since many lines of different ionization states of carbon, helium, oxygen and silicon are seen, frequently combined into difficult blends (Fig. 4). The effects of changes of ionization state in the envelopes with the spectral subtype are easily seen, mainly in carbon lines. As we go from early to late subtypes, one

can notice the continuous change in intensity of CIV λ 1551 and HeII λ 1640 lines. Much stronger in WC 5 carbon line becomes of the same intensity as HeII λ 1640 in WC 7 then disappears quickly and in WC 9 is hardly seen. Both these lines, however, are decreasing their intensity (EW) as going from early to late WC subtypes.

The next easily seen effect is the systematic increase of intensity of CIII lines, most clearly represented by CIII λ 2297 and CIII λ 1909, relative to CIV. These lines become well seen in WC 7, but in WC 8 and WC 9 they form the strongest spectrum.

Also the CII λ 2837 line becomes stronger as going from WC 5 to WC 9, where it is one of the strongest lines (after CIII). Because of a variety of emission lines observed in UV spectra of WC stars, one can also follow changes of relative intensity of lines of oxygen (for instance OIV λ 3070 and OV λ 3130) or silicon. The λ 2530 blend exhibits an interesting behavior – most prominent component seem to change with spectral subtype. This blend, as seen in IUE low resolution, is probably composed of CIV λ 2524 and λ 2530, CII λ 2509 and λ 2512, SiIII λ 2542 and SiIV λ 2517.

The equivalent widths of many strong lines seen in ultraviolet spectra of WC stars correlate well with spectral subtype as it is shown in Figs. 8 and 9. From these figures one can also easily notice that WC stars form (as frequently concluded before) a much more uniform group than the WN. As it can be seen in Fig. 8 CIII λ 1909 is very weakly or not at all correlated with spectral subtype of WC stars, while other strong lines, such as C IV λ 1551, HeII λ 1640 or CII λ 2837 (their equivalent widths), are very well correlated with spectral subtype (r=−0.92 for CIV). In Fig. 8f the equivalent width of the λ 2530 blend, discussed above, are plotted vs. spectral subtype.

Also line ratios presented in Fig. 9a-c correlate very well with spectral subtype. The trend of higher ionization toward earlier subtypes is plainly pronounced, r=0.89 and 0.92 for CII to CIII and CIII to CIV respectively, while for CII to CIV it attains the value of 0.98.

Looking for comparisons between galactic and LMC WC stars, one should start from WC 5 stars, since they are present in this study in almost the same quantity. From Fig. 8c,d one could conclude, as it was in case of WN stars, that LMC stars seem to have stronger line spectrum or, if to be more precise, among stars with strongest lines LMC stars seem to be more frequent.

5. Line widths

Since in our study we have not restricted ourselves to measuring equivalent widths and line fluxes but we also measured line widths (FWHM), we have now a unique possibility to follow changes of line widths for many emission lines in a number of galactic and LMC WR stars. FWHM were measured for all emission lines, here however, we will discuss only relations concerning most prominent lines in both WN and WC stars.

5.1. *WN stars*

In Fig. 10a-d we can see FWHM of HeII λ 3203, HeII λ 1640, CIV λ 1551 and NIV λ 1486 plotted versus spectral subtype of WN stars. These figures show the representative scatter of emission line widths when plotted vs. spectral subtype. It is most evident in the case of HeII λ 3203 and NIV λ 1486. For these two lines, the line widths (FWHM) for a given subclass may differ 3-4 times. On two other graphs from that panel we can see that the HeII λ 1640 and CIV λ 1550 FWHM show some correlation with WN spectral subtype. In both cases the line widths seem to decrease while moving from early to late type WN stars.

One can also notice the similarity of widths of galactic and LMC WN stars. These figures also show that the scatter present in EW data is present in FWHM of emission lines of WN stars as well – the FWHM data confirm the composed nature of WN class.

5.2. *WC stars*

Figure 11a-d shows several plots of emission line widths (FWHM) vs. spectral subtype for galactic and LMC WC stars. In Fig. 11a we can see a lack of correlation of widths of HeII line, λ 3203, with spectral subtype. Also other line widths, not shown here, such as HeII λ 1640 and CII λ 1247 are uncorrelated with spectral subtype. Other figures from that panel show, however, a surprisingly strong correlation with spectral subtype of WC stars.

In the case of CIV λ 1551 the correlation is most prominent $r = -0.84$, and we can easily see that the line widths decrease while going to later subtypes, with scatter being relatively small. Only the stars of the WC 6 subclass exhibit substantial differences in CIV λ 1550 line widths, the mean value, however, lies correctly on the slope determined by other data.

Also the CIII λ 1909 line widths correlate well with spectral subtype. We can see also a decrease of FWHM with spectral subtype of WC stars. The scatter, however, is larger.

The OV λ 1375 line data show an increase of line widths with spectral subtype, at least for WCL stars. The FWHM data for WC 5 stars seem to suggest that this relation may fail for WNE stars.

Figure 11 shows that the line widths of galactic and LMC WC stars do not differ substantially.

6. Emission line relations

In Tables 6a,b,c,d observed central wavelengths, equivalent widths, FWHM and the observed line fluxes are given for most prominent (described in Sect. 3) lines seen in the

UV spectra of WR stars. Many emission line relations between UV lines and UV vs. optical (from Conti et al. 1983; Conti & Massey 1989) or NIR (from Conti et al. 1990) are possible to draw, on the basis of our and literature data. The most interesting of them are shown in Figs. 12 and 13 for WN and Figs. 14, 15 and 16 for WC's.

6.1. *WN stars*

In Fig. 12a,b,c and d we can see a correlation between equivalent widths of HeII lines from IUE, optical and NIR regions. As it is shown in Fig. 12a for λ 3203 (5-3) and λ 2733 (6-3) close lines of one series are very well correlated (r=0.98). Similar effect is seen in Fig. 12b for λ 4686 (4-3) and λ 3203 (5-3). Such correlation is weaker, if to include HeII λ 1640 (3-2) because of strong influence of P Cygni absorption component - Fig. 12c. If to use lines from different, distant, wavelength regions, as it is shown in Fig. 12d for λ 10124 (5-4) and λ 2733 (6-3) the correlation becomes still weaker. This probably reflects the influence of envelope optical depth for line radiation. A comparison between theoretical and observed HeII lines is given in Schmutz (1991).

In Fig. 13a,b,c we can see some relations between equivalent widths of some more emission lines seen in WN stars spectra. In Fig. 13a a correlation between two NIV lines, namely λ 1486 and λ 3480 is shown. These lines intensities (EW) do not correlate at all in WNL stars which is a reflection of different processes controlling their intensity: the former being very electron temperature dependent and driven by collisional process while the later – abundance sensitive and produced by indirect fluorescence (Hillier 1988). In the case of WNE a correlation of EW of these lines is well seen. In Fig. 13b we can see a strong correlation between NIV λ 1486 and CIV λ 1551 (r=0.88).

Looking at different line-line relations we can also find a systematic effect showing that between stars with strongest emission lines LMC WN stars are more numerous.

6.2. *WC stars*

Figures 14a,b for WC stars are the counterparts of Figs. 12a,c for WN stars. They show correlations between EW of HeII lines from different spectral regions. We have no optical data for HeII λ 4686, as in WC stars rather CIII/CIV/HeII feature was observed (Torres et al. 1986; Conti & Massey 1989) in which CIII λ 4650 is the leading line – thus we could not construct the counterpart of Fig. 12b. Figures 12a,c and 11a,b are plot in the same scale, the latter ones complement very well the former ones and supply the conclusion drawn in Sect. 6.1.

In Fig. 15 an equivalent widths of two CIII emissions from UV (λ 1909) and optical (λ 5696) data are compared. One can easily notice that the correlation between equivalent widths of these lines is rather weak. This is simply a reflection of small changes of EW of the former line. Only the late type stars seem to form a kind of relation in this graph.

A similar effect can be seen in Fig. 15b where EW of CIII λ 1909 are compared to those of CIV λ 1550. Although both these lines should be driven by collisional excitations (Hillier 1989) and behave in a similar manner, their EW do not correlate. This is most probably connected with the serious blending of CIII λ 1909 by CIII λ 1923 (Hamann et al. 1992). We obtain nearly the same picture when we plot equivalent widths of SiIV λ 1725 vs. CIV λ 1550 - Fig. 15c. Another figure of this series shows a strong correlation of CIV λ 1550 with CII λ 2837 (Fig. 15d) and OIII-V λ 5592 with OIII λ 3130 blend – Fig. 15e. In this figure we can also see that the latter line correlates relatively well with CIV λ 1550 – Fig. 15f.

6.3. *WN and WC stars*

Because of the presence of some lines both in WN and WC spectra, we can study some line-line (equivalent width) relations for WN and WC stars together. Of such common to WN and WC stars the λ 1551 and λ 5808 CIV and unblended (in WC stars) HeII lines are most prominent. In Fig. 16a we can follow the run of one of those line pairs basing only on UV lines. The CIV λ 1551 emission line EW as a function of EW of HeII λ 1640 shows strong distinction between WN and WC stars. There are two different, clearly seen, relations and only Galactic WNL stars are located between them, in origin of "horns". For galactic and LMC WC stars we have

log EW (1551)=1.08(±0.13) × log EW(1640) + 0.18 (± 0.21)

with r=0.95,

while for WNE

log EW (1551)=0.74(±0.08) × log EW(1640) −0.18 (± 0.13)

with r=0.90.

The WNL stars are scattered on this graph. Most of them appear in the origin of both WC and WNE sequences, some others, however, lie on the linear relation defined by WNE stars.

Another, similar diagram may be constructed basing on CIV λ 1551 and λ 5808 lines alone - Fig. 16b. The separation between WN and WC sequences is not so evident. All WN stars are located (as expected) close to WCE stars. Both WC and WN stars form, however, well defined linear sequences in this graph.

Figure 16c is simply a copy of Fig. 16a. with CIV λ 1551 replaced by CIV λ 5808. The parallel WN and WC sequences are even better separated, and seem to be more linear.

The interpretation of these figures is not so evident since the emission lines driving mechanisms can differ in WN and WC stars.

Since in this study we are mainly interested in "single" WR stars no bright composed WN+WC stars were analyzed and we cannot draw any conclusion on their position in such graphs as given above. The only example of such composed-spectrum objects we analyzed here is Br29 (WN3/WCE). As it can be seen in Figs. 16a-c it behaves like a WC star, as noted already in Conti & Massey (1989) on the basis of λ 4686 HeII vs. λ 5808 CIV graph. Figure 16 a confirms that this composed-spectrum effect is seen also in UV spectrum of Br29 (using the classification criteria, given in the following section, based on the λ 1551 CIV EW and FWHM we can classify the WC spectrum of this star as WC 5-7).

7. Spectral classification in ultraviolet

The spectra gathered here cover all subtypes of WN stars and a wide range of WC stars. We collected data for over 30% of all galactic WR stars and many from LMC. We may, therefore, look for classification criteria of WR stars in the ultraviolet region alone. For that purpose, we will use the equivalent width (EW) and line width (FWHM) data, as described in Sects. 4-6. Since in every sense the WC stars, although having more complicated spectra, appear more uniform let us start with them.

7.1. *WC stars*

The optical spectral classification of WC stars (Beals & Plaskett 1935; Smith 1968) is based on the yellow region $\lambda\lambda$ 5500 – 5900 Å. It is based on strengths of two carbon lines, namely CIII λ 5696 and CIV λ 5808, both difficult to model (Hillier 1989; Hamann et al. 1992) supplemented by OIII-V λ 5592.

In our study we showed already that the strengths (EW) of CIV λ 1551, CII λ 2837 and HeII λ 1640 correlate well with spectral subtype of WC stars. Also the line widths (FWHM) of CIV λ 1551, OV λ 1375 and CIII λ 1909 allow us to predict spectral type of WC stars. Moreover some line–line relations such as CIV λ 1551/CII λ 2837 can be used for that purpose. Even if to reject the HeII λ 1640, as blended with CIV and possibly influenced by P Cygni absorption, and OV λ 1375, we still have a variety of criteria for UV classification of WC stars.

The most promising of them offers CIV λ 1551 line, the strongest in most of these stars in the UV. This line is created by collisional excitation (Hillier 1989) and controls temperature structure of the stellar wind. Its intensity is well reproduced by models (Hillier 1989; Hamann et al. 1992). For this line the FWHM data alone can be used to reproduce spectral subtype of WC star. Using our data as showed in Fig. 11b, we can obtain spectral subtype of a galactic and LMC WC star by taking the integer part of the equation

$$\mathrm{Sp^{WC}} = -0.21(\pm 0.03) \times \mathrm{FWHM\ (CIV\ 1551)[\AA]} + 9.63(\pm 0.48)$$

This equation allows one to obtain spectral subtype with an accuracy of one subclass in most cases. We found only two exceptions: WR 14 and 15. For these stars the difference between the commonly adopted, WC 6, and determined here spectral subclass is 2. Both these stars according to the above-given criterion would be WC 4 stars because of their large width of CIV λ 1551 line as determined here. However, as showed in Fig. 11b, the scatter of CIV λ 1550 line widths of WC 6 subclass is the highest.

Basing on equivalent width data for this line (Fig. 8c) we obtain another criterion:

$$\mathrm{Sp^{WC}} = -2.94(\pm 0.17) \times \mathrm{Log\ EW\ (CIV\ 1551)[\AA]} + 11.44(\pm 0.80)$$

which allows us to determine spectral subtype with not more than one subclass error ($r = -0.92$). Similar relations can be found for CII λ 2837 (r=77).

Another group of criteria comes from Figs. 9a-c. Using for instance the CII λ 2837 and CIV λ 1551 lines we obtain:

$$\mathrm{Sp^{WC}} = 1.95(\pm 0.01) \times \frac{\mathrm{Log\ EW\ (CII\ 2837)}}{\mathrm{Log\ EW\ (CIV\ 1551)}} + 7.70(\pm 0.04)$$

We may conclude that basing on low resolution spectra of WC stars alone, we were able to reproduce spectral subtypes for WC 5-9 stars with precision of one subclass in most cases, using the above, simple criteria.

Another interesting conclusion, connected with spectral classification of WC stars, is that the smooth run of equivalent widths of CIV λ 1551 with spectral subtype of WC stars suggests that the classification scheme of these objects reproduces the electron temperature variations in their envelopes since the CIV λ 1551 line strength is mainly controlled by electron temperature according to Hillier (1989).

7.2. *WN stars*

Optical classification of WN stars (Beals & Plaskett 1935; Smith 1968) is based upon the intensities of nitrogen and helium lines mainly in the range of $\lambda\lambda$ 4000 – 4700 Å. Of nitrogen lines NIII $\lambda\lambda$ 4634-40 (blend) and λ 5314, NIV λ 3480 and λ 4058, NV λ 4604, λ 4620 and $\lambda\lambda$ 4933-44 (blend) are used. Some of these lines were modeled by Hillier (1988): NV λ 4604, NIV λ 4058, NIV λ 3480. Their intensity and shape is not well reproduced and variety of line driving mechanisms is proposed by Hillier (1988). The use of these lines suggest that so defined spectral types have little to do with physics of WN stars.

In this paper several UV lines of nitrogen and helium were measured in the spectra of WN stars. Their EW and FWHM correlations with spectral subtype were studied in Sects. 4-6. Let us summarize these results.

The line widths of most prominent emission lines in WN stars do not correlate well with spectral subtype, they cannot be useful for spectral classification. Equivalent widths of NIII λ 1750 line correlate relatively well with WN spectral type, but the scatter in this relation makes it useless for spectral classification. The same concerns NV λ 1241 and the UV HeII lines.

Using line-line (EW) relations for NIII λ 1750/NIV λ 1486, NIV λ 1486/NV λ 1241 or NIII λ 1750/NV λ 1241, we may obtain some kind of EW ratio vs. spectral type for WN stars but again, the scatter does not allow us to reproduce spectral types of these stars with reasonable accuracy.

Let us here point out an interesting behavior of NIV λ 1486, CIV λ 1551 and HeII λ 1640 equivalent widths. All these lines, in spite of large scatter of EW for a given spectral type, show similar tendency of increasing EW for early WN (WNE) types and decreasing EW for WNL, with a maximum around WN 4 - 5. This is even more interesting since according to Hillier (1988) at least two of these lines, CIV λ 1551 and NIV λ 1486, are very electron temperature sensitive. This fact together with Figs. 5b,d and 6 a suggest that the classification scheme for WN stars is very weakly or not at all connected to temperature in WN envelopes. These figures seem to suggest rather that within the WN sequence we deal with two opposite electron temperature sequences: one from WN 2 to WN 4-5 and the second from WN 4-5 to WN 8.

8. Conclusions

We presented a large, representative, complete to $v = 12$ sample of ultraviolet spectra of "single" galactic and LMC WR stars, basing on the International Ultraviolet Explorer Archive. The presented material enables us to draw the following conclusions:

1. The spectral effects of changing physical conditions in WR envelopes are well seen in their UV spectra.
2. The ultraviolet spectra of WR stars mimic very well their optical and NIR spectra. The WC stars in spite of their extremely complicated spectra, seem to form a more uniform group, while the WN spectra show large scatter of equivalent widths (as stated before in Conti et al. 1983; Torress et al. 1986) and line widths (FWHM) within one subtype.
3. The comparison of emission lines of the same ion at distant wavelengths shows that the influence of the envelope on the line radiation plays an important role in WR stars.
4. Ultraviolet spectra of LMC and galactic stars do not seem to be identical. In several cases, as for instance HeII λ 1640, the LMC WN stars show stronger (in terms of EW) lines while in some other ones LMC stars more frequently have strongest lines.
5. Based on low resolution IUE spectra alone, we were able to reproduce spectral classification of WC stars basing, in principle, on one line - CIV λ 1551 - equivalent widths and FWHM.
6. The shape of relation for EW of CIV λ 1551, NIV λ 1486 and HeII λ 1640 in WN stars suggests that within WN stars we are dealing with two electron temperature sequences.
7. It is concluded that not only the equivalent widths, but also the rarely measured line width (FWHM) carry on important information concerning WR envelopes.
8. More IUE spectra of galactic and LMC Wolf-Rayet stars are needed since for some of the stars under consideration here the spectra are of poor quality, especially around the 2200 bump, where the fluxes are the smallest.

Acknowledgements. The important comments of the referee, P. Crowther are acknowledged with thanks. We also thank Zbroja for kindly improving the English of the manuscript. This work was supported by the Polish Committee for Science Research (KBN) under the grant No. 2 2112 92 03 through N. Copernicus University in Toruń.

References

Barlow M.J., Hummer D.G. 1982, in "Wolf-Rayet Stars: Observations, Physics, Evolution" IAU Symp. 99 (eds. W.H. de Loore and A.J. Willis) 387
Beals C.S., Plaskett H.H. 1935, Trans. IAU 5, 184
Bohlin R.C., Holm A.V. 1980, NASA IUE Newsletter 10, 37
Boggess A. et al. 1978a, Nature 275, 372
Boggess A. et al. 1978b, Nature 275, 377
Borkowski J. 1992, "ReWiA 2.0 - user's manual" (in Polish) PAI CAMK PAN Toruń
Conti P.S., Leep E.M., Perry D.N. 1983, ApJ 268, 288
Conti P.S., Massey P. 1989, ApJ 337, 251
Conti P.S., Massey P., Garmany C.D. 1989, ApJ 341, 113
Conti P.S., Massey P., Vreux J.-M. 1990, ApJ 354, 359
Hamann W.-R., Leuenhagen U., Koesterke L., Wessolowski U. 1992, A&A 255, 200
Hillier D.J. 1987, ApJS 63, 965
Hillier D.J. 1988, ApJ 327, 822
Hillier D.J. 1989, ApJ 347, 392
van der Hucht K.A., Hidayat B., Admiranto A.G., Supelli K.R., Doom C. 1988 A&A 199, 217
van der Hucht K.A. 1992, A&AR 4, 123
Koenigsberger G. 1990, A&AS 235, 282
Massey P. 1984, APJ 281, 789
Nugis T. 1991, in "Evolution of stars: the Photospheric Abundance Connection" IAU Symp. 145, eds. G. Michaud, A. Tutukov, 209
Nussbaumer H., Schmutz W., Smith, L.J., Willis A.J. 1982, A&AS 47, 257

Schmutz W. 1991, in "Wolf - Rayet Stars and Interrelations with other massive stars in galaxies" IAU Symp 143, eds. K.A. van der Hucht and B. Hidayat (Kluwer) 39
Smith L.F. 1968, MNRAS 138, 109
Smith L.J., Willis A.J. 1983, A&AS 54, 229
Striganow A.R., Odincowa G.A. 1982, "Tables of spectral lines of atoms and ions" (in Russian) Energizdat, Moscow
Torres A.V., Conti P.S. 1984, ApJ 280, 181
Torres A.V. 1985, Thesis, JILA, Colorado
Torres A.V., Conti P.S., Massey P. 1986, ApJ 300, 379
Torres-Dodgen A.V., Massey P. 1988, AJ 96, 1076
Underhill A.B. 1991, in "Wolf - Rayet Stars and Interrelations with other massive stars in galaxies" IAU Symp 143, eds. K.A. van der Hucht and B. Hidayat (Kluwer) 53
Vreux J.M., Dennefeld M., Andriliat Y. 1983, A&AS 54, 437
Vreux J.-M., Andrilliat Y., Biemont E. 1990, A&A 238, 207
Willis A.J. 1980, in "Proc. 2nd European IUE Conf.", ESA SP-157
Willis A.J., van der Hucht K.A., Conti P.S., Garmany C.D. 1986, A&AS 63, 417
Wolf C.J.E., Rayet G.A.P 1867, Comptes Rendu 65, 292

Table 3. Subtype distribution of program stars relative to all known WR stars in the Galaxy and LMC, respectively

Subtype	2	3	4	4.5	5	6	7	8	9	Σ	%
WN Galaxy	1	8	13	7	6	24	22	11	1	93	
this work	1	2	3	3	3	8	9	4	1	34	35
WN LMC		29	22	3	5	6	9	4	3	81	
this work		13	6	0	2	1	6	1	2	31	38
WC Galaxy			5		11	15	13	9	18	73	
this work			0		5	6	4	2	5	22	30
WC LMC					17	1				18	
this work					6	1				7	39

Table 4. Observational material

Star WR	Camera	Image nr	A	Exp. [sec]	Camera	Image nr	A	Exp. [sec]
1	SWP	09758	LAP	1500	LWR	08476	LAP	2100
	SWP	13909	LAP	1200	LWR	08477	LAP	600
2	SWP	06947	LAP	599	LWR	16222	LAP	540
	SWP	20303	LAP	720	LWP	09543	LAP	6600
3	SWP	04311	LAP	140	LWR	16217	LAP	180
	SWP	04311	SAP	210				
	SWP	20293	LAP	300				
4	SWP	10726	LAP	480	LWR	09421	LAP	480
	SWP	04310	LAP	300	LWR	03807	LAP	240
	SWP	04310	SAP	480	LWR	03807	SAP	360
5	SWP	10725	LAP	2700	LWR	09420	LAP	2400
	SWP	11123	LAP	2100	LWR	09751	LAP	1200
6	SWP	04064	LAP	10	LWR	03603	LAP	8
	SWP	04064	SAP	6	LWR	03603	SAP	4
	SWP	13844	LAP	3	LWR	08788	LAP	7
	SWP	13844	SAP	4	LWR	10476	LAP	12
	SWP	14136	LAP	5				
	SWP	14136	SAP	2				
7	SWP	03541	LAP	2700	LWR	03114	LAP	1500
	SWP	03541	SAP	1500	LWR	03114	SAP	600
10	SWP	10748	LAP	780	LWR	09439	LAP	600
	SWP	13912	LAP	1020	LWR	10538	LAP	660
12	SWP	10749	LAP	1800	LWR	14562	LAP	2880
	SWP	18473	LAP	2400	LWP	17554	LAP	1080
14	SWP	10087	LAP	180	LWR	05876	LAP	149
	SWP	10104	LAP	500	LWR	05876	SAP	149
	SWP	10106	LAP	714	LWR	08786	LAP	714

Star WR	Camera	Image nr	A	Exp. [sec]	Camera	Image nr	A	Exp. [sec]
15	SWP	31396	LAP	5100	LWP	11272	LAP	3600
	SWP	33590	LAP	6000	LWP	13285	LAP	4800
16	SWP	04333	LAP	80	LWR	03827	LAP	58
	SWP	04333	SAP	160	LWR	03827	SAP	116
	SWP	06970	LAP	89				
	SWP	06970	SAP	89				
17	SWP	10713	LAP	480	LWR	09436	LAP	300
	SWP	10756	LAP	360	LWP	18185	LAP	180
	SWP	39142	LAP	240				
18	SWP	09185	LAP	3060	LWR	07789	LAP	1800
	SWP	10714	LAP	1860	LWR	09753	LAP	480
					LWR	10478	LAP	720
22	SWP	04066	LAP	11	LWR	03604	LAP	10
	SWP	04066	SAP	6	LWR	03604	SAP	6
	SWP	16083	LAP	6	LWR	12382	LAP	5
23	SWP	07027	LAP	159	LWR	05955	LAP	79
	SWP	07027	SAP	159	LWR	05955	SAP	79
	SWP	11280	LAP	120				
	SWP	11280	SAP	150				
24	SWP	01634	LAP	5.5	LWR	03825	LAP	3
	SWP	01634	SAP	5.5	LWR	03825	SAP	5.5
	SWP	04331	LAP	3.5				
	SWP	04331	SAP	5				
25	SWP	02709	LAP	120	LWR	02419	LAP	120
	SWP	02709	SAP	120	LWR	13343	LAP	120
	SWP	17065	LAP	120	LWR	14563	LAP	105
33	SWP	18467	LAP	1800	LWR	14558	LAP	1440
	SWP	18474	LAP	2400				

Table 4. continued

Star WR	Camera	Image nr	A	Exp. [sec]	Camera	Image nr	A	Exp. [sec]
40	SWP	04068	LAP	30	LWR	05099	LAP	80
	SWP	04068	SAP	15	LWR	05099	SAP	45
	SWP	05851	LAP	80	LWR	05112	LAP	80
	SWP	05851	SAP	55	LWR	05112	SAP	45
					LWR	05877	LAP	80
					LWR	05877	SAP	45
44	SWP	18466	LAP	6000	LWR	14557	LAP	6000
50	SWP	11125	LAP	6000	LWR	09752	LAP	3300
52	SWP	06974	LAP	419	LWR	05918	LAP	159
	SWP	06974	SAP	419	LWR	05918	SAP	159
	SWP	39140	LAP	120				
53	SWP	13897	LAP	660	LWR	10525	LAP	420
55	SWP	10750	LAP	1320	LWR	07786	LAP	1140
	SWP	13896	LAP	1320	LWR	10524	LAP	900
56	SWP	09184	LAP	10800	LWR	07941	LAP	7200
	SWP	10932	LAP	15300				
57	SWP	06975	LAP	159	LWP	18177	LAP	60
	SWP	06975	SAP	159				
	SWP	39139	LAP	120				
61	SWP	09187	LAP	1800	LWR	07944	LAP	2760
	SWP	10933	LAP	6300	LWP	17623	LAP	1200
69	SWP	13899	LAP	420	LWR	05419	LAP	225
	SWP	25314	LAP	410	LWR	10527	LAP	240
	SWP	25315	LAP	300	LWP	18176	LAP	80
71	SWP	09761	LAP	480	LWR	08481	LAP	240
	SWP	09761	SAP	300	LWR	08481	SAP	300
75	SWP	09186	LAP	3000	LWR	07943	LAP	3600
	SWP	11124	LAP	6000	LWP	17621	LAP	1800

Star WR	Camera	Image nr	A	Exp. [sec]	Camera	Image nr	A	Exp. [sec]
78	SWP	04335	LAP	11	LWR	03829	LAP	7
	SWP	04335	SAP	22	LWR	03829	SAP	15
85	SWP	41427	LAP	3000	LWP	20192	LAP	1080
86	SWP	23403	LAP	960	LWP	03711	LAP	1500
	SWP	25312	LAP	1440	LWP	05417	LAP	552
90	SWP	25313	LAP	10	LWR	03830	LAP	10.5
					LWR	03830	SAP	21
					LWP	05418	LAP	11
92	SWP	06937	LAP	719	LWR	05894	LAP	539
	SWP	06937	SAP	719	LWR	05894	SAP	539
103	SWP	02845	LAP	120	LWR	02531	LAP	120
	SWP	02845	SAP	120	LWR	02531	SAP	120
	SWP	04337	LAP	90	LWR	03874	LAP	60
	SWP	04337	SAP	180	LWR	03874	SAP	120
104	SWP	31395	LAP	2820	LWP	11271	LAP	6000
106	SWP	33591	LAP	4320	LWP	13286	LAP	3600
108	SWP	38443	LAP	3000	LWP	17620	LAP	1080
110	SWP	09760	LAP	2100	LWR	08479	LAP	1800
	SWP	38442	LAP	300	LWR	17619	LAP	900
111	SWP	02847	LAP	20	LWR	03809	LAP	9
	SWP	02847	SAP	20	LWR	03809	SAP	14
	SWP	04313	LAP	6				
	SWP	04313	SAP	9				
123	SWP	14138	LAP	2400	LWR	10530	LAP	600
	SWP	14716	LAP	4200	LWR	10758	LAP	2400
128	SWP	04398	LAP	120	LWR	03873	LAP	75
	SWP	04398	SAP	240	LWR	03873	SAP	150

Star WR	Camera	Image nr	A	Exp. [sec]	Camera	Image nr	A	Exp. [sec]
134	SWP	04087	LAP	120	LWR	03626	LAP	240
	SWP	04087	SAP	60	LWR	06161	LAP	50
	SWP	07161	LAP	30	LWR	06161	SAP	300
	SWP	07161	SAP	60				
135	SWP	02842	LAP	60	LWR	03622	LAP	120
	SWP	02842	SAP	60	LWR	03622	SAP	60
	SWP	04085	LAP	100	LWP	18174	LAP	20
	SWP	04085	SAP	50				
136	SWP	21811	LAP	40	LWR	03806	LAP	30
	SWP	21811	SAP	25	LWR	03806	SAP	240
	SWP	21823	LAP	40	LWR	08478	LAP	120
	SWP	21823	SAP	25	LWR	08478	SAP	39
138	SWP	15583	LAP	300	LWP	10516	LAP	840
	SWP	17062	LAP	135	LWR	13340	LAP	120
141	SWP	16080	LAP	2520	LWR	12379	LAP	1860
148	SWP	14171	LAP	2400	LWR	10755	LAP	720
	SWP	14713	LAP	3000	LWR	12431	LAP	720
152	SWP	17063	LAP	1800	LWR	13341	LAP	1800
	SWP	18450	LAP	1500	LWR	14546	LAP	1440
154	SWP	17079	LAP	1020	LWR	13364	LAP	1140
155	SWP	06070	LAP	300	LWR	05951	LAP	374
	SWP	10136	LAP	360	LWR	05951	SAP	180
	SWP	10138	LAP	360	LWR	05952	LAP	120
					LWR	10617	LAP	120
156	SWP	18465	LAP	6600	LWR	14556	LAP	5400
157	SWP	17078	LAP	840	LWR	13363	LAP	1020
158	SWP	39432	LAP	8100	LWP	18548	LAP	2700

Star Br	Camera	Image nr	A	Exp. [sec]	Camera	Image nr	A	Exp. [sec]
1	SWP	23384	LAP	7200	LWP	03699	LAP	6000
	SWP	33443	LAP	21600				
3	SWP	33445	LAP	7200	LWP	17628	LAP	4800
	SWP	33446	LAP	1200				
6	SWP	04134	LAP	1800	LWR	03665	LAP	1200
7	SWP	04090	LAP	3600	LWR	03628	LAP	3600
	SWP	04092	LAP	1200				
8	SWP	04117	LAP	2400	LWR	03647	LAP	2820
	SWP	07582	LAP	2100	LWR	06557	LAP	3600
10	SWP	14161	LAP	1200	LWR	10767	LAP	1020
	SWP	14162	LAP	480				
12	SWP	10751	LAP	1920	LWR	07915	LAP	3600
	SWP	18451	LAP	1920	LWR	14547	LAP	1500
13	SWP	04093	LAP	600	LWR	03630	LAP	720
	SWP	04364	LAP	720	LWR	03841	LAP	900
14	SWP	04365	LAP	1560	LWR	03842	LAP	1380
15	SWP	38236	LAP	840	LWP	17416	LAP	2700
	SWP	38247	LAP	2700				
18	SWP	06197	LAP	330	LWR	04172	LAP	480
	SWP	10729	LAP	1020	LWR	05361	LAP	480
	SWP	18452	LAP	1020				
19	SWP	07003	LAP	2700	LWP	13165	LAP	1380
	SWP	33447	LAP	6000				
23	SWP	09169	LAP	3600	LWR	07916	LAP	3600
	SWP	10710	LAP	5580				

Table 4. continued

Star Br	Camera	Image nr	A	Exp. [sec]	Camera	Image nr	A	Exp. [sec]
24	SWP	04832	LAP	1440	LWR	04175	LAP	1800
	SWP	06185	LAP	660	LWR	05350	LAP	1200
25	SWP	33454	LAP	18000	LWP	17629	LAP	9300
	SWP	33455	LAP	2700				
26	SWP	06186	LAP	540	LWR	05351	LAP	780
	SWP	09162	LAP	720	LWR	07909	LAP	720
27	SWP	23387	LAP	2400	LWP	03702	LAP	3000
35	SWP	38451	LAP	600	LWP	20197	LAP	3780
38	SWP	23385	LAP	5100	LWP	03700	LAP	5400
40	SWP	23398	LAP	2700	LWP	03707	LAP	3000
43	SWP	04366	LAP	1740	LWR	03649	LAP	1800
	SWP	04836	LAP	1500	LWR	03843	LAP	2640
46	SWP	38249	LAP	900	LWP	17418	LAP	2700
50	SWP	04135	LAP	1020	LWR	03666	LAP	1200
	SWP	06188	LAP	1020	LWR	05353	LAP	1620
56	SWP	38234	LAP	2100	LWP	17415	LAP	1800
58	SWP	23891	LAP	7200	LWP	04163	LAP	4500
59	SWP	10711	LAP	1620	LWR	13345	LAP	1260
	SWP	18469	LAP	900	LWR	14560	LAP	1500
62	SWP	07579	LAP	900	LWR	06555	LAP	1680
	SWP	39144	LAP	4800	LWP	18179	LAP	3600
64	SWP	23400	LAP	1200	LWP	17417	LAP	600
	SWP	23890	LAP	3360				

Star Br	Camera	Image nr	A	Exp. [sec]	Camera	Image nr	A	Exp. [sec]
71	SWP	23399	LAP	2700	LWP	03708	LAP	2400
80	SWP	10701	LAP	1020	LWR	09434	LAP	960
89	SWP	13981	LAP	300	LWR	02494	LAP	360
	SWP	13981	SAP	300	LWR	02494	SAP	360
					LWR	10629	LAP	360
					LWR	10629	SAP	360
90	SWP	04138	LAP	360	LWR	03669	LAP	480
	SWP	06189	LAP	720	LWR	05354	LAP	720
	SWP	14005	LAP	1800	LWR	11562	LAP	900
					LWR	11562	SAP	780
92	SWP	04139	LAP	900	LWR	03670	LAP	1080
93	SWP	04191	LAP	3000	LWR	06556	LAP	3600
	SWP	07581	LAP	3600				
98	SWP	09910	LAP	1800	LWR	08623	LAP	2700
99	SWP	23386	LAP	3300	LWP	03701	LAP	3900
					LWP	04162	LAP	3600
100	SWP	04137	LAP	3000	LWR	03668	LAP	3600
	SWP	09911	LAP	2400	LWR	08624	LAP	3000
	SWP	09912	LAP	1500				

Table 5. Finding list of the strongest UV lines present or possibly present in low resolution IUE spectra of WR stars (based on Striganow & Odincowa 1982): a) helium HeI, HeII, b) nitrogen NIII, NIV, NV, c) oxygen OIV, OV, OVI, d) carbon CII, CIII, CIV, e) oxygen OIII and silicon SiIII, SiIV

He I			He II		
λ	I_{lab}	Transition	λ	I_{lab}	Transition
			1215.134	7	$2p^2P^0 - 4d^2D$
			1640.417	15	$2p^2P^0 - 3d^2D$
			2165.248	2	$3d^2D - 13f^2F^0$
			2186.604	4	$3d^2D - 12f^2F^0$
			2214.671	6	$3d^2D - 11f^2F^0$
			2252.689	10	$3d^2D - 10f^2F^0$
			2306.194	20	$3d^2D - 9f^2F^0$
			2385.404	30	$3d^2D - 8f^2F^0$
			2511.205	50	$3d^2D - 7f^2F^0$
2644.802	2	$2s^3S - 13p^3P^0$			
2652.848	3	$2s^3S - 12p^3P^0$			
2663.271	4	$2s^3S - 11p^3P^0$			
2677.135	5	$2s^3S - 10p^3P^0$			
2696.119	7	$2s^3S - 9p^3P^0$			
2723.191	10	$2s^3S - 8p^3P^0$			
			2733.297	100	$3d^2D - 6f^2F^0$
2763.804	20	$2s^3S - 7p^3P^0$			
2829.076	40	$2s^3S - 6p^3P^0$			
2945.106	100	$2s^3S - 5p^3P^0$			
3187.745	200	$2s^3S - 4p^3P^0$			
			3203.102	200	$3d^2D - 5f^2F^0$

Table 5. continued

N III			N IV			N V		
λ	I_{lab}	Transition	λ	I_{lab}	Transition	λ	I_{lab}	Transition
			1133.1	4	$3s\ ^3S - 3s'\ ^3P^0$			
			1135.2	3	$3s\ ^3S - 3s'\ ^3P^0$			
			1168.6	3	$3d\ ^3D - 3d'\ ^3D^0$			
1183.0	14	$2p^2\ ^2P - 2p^3\ ^2P^0$						
1184.5	15	$2p^2\ ^2P - 2p^3\ ^2P^0$						
			1188.0	6	$3s\ ^1S - 3s'\ ^1P^0$			
			1225.2	3	$3p\ ^3P^0 - 4s\ ^3S$			
			1225.7	4	$3p\ ^3P^0 - 4s\ ^3S$			
						1238.8	20	$2s\ ^2S - 2p\ ^2P^0$
						1242.8	19	$2s\ ^2S - 2p\ ^2P^0$
			1270.3	5	$3p\ ^3P^0 - 3p'\ ^3D$			
			1272.2	4	$3p\ ^3P^0 - 3p'\ ^3D$			
			1273.5	3	$3p\ ^3P^0 - 3p'\ ^3D$			
			1284.2	3	$3d\ ^1D - 4p\ ^1P^0$			
			1296.6	5	$3d\ ^1D - 3d'\ ^1F^0$			
			1309.6	4	$3p\ ^1P^0 - 3p'\ ^1P$			
1387.4	8	$3p\ ^2P^0 - 4d\ ^2D$						
						1389.5	3	$4s\ ^2S - 5p\ ^2P^0$
						1389.8	2	$4s\ ^2S - 5p\ ^2P^0$
			1438.4	3	$3d'\ ^1F^0 - 6g\ ^1G$			
			1446.1	5	$3d\ ^1D - 3d'\ ^1D^0$			
			1486.5	2	$2s^2\ ^1S - 2p\ ^3P^0$			
						1495.5	2	$5fgh - 8ghi$
						1549.3	6	$4p\ ^2P^0 - 5d\ ^2D$
1471.7	5	$3p'\ ^4P - 4d'\ ^4D^0$						
1575.2	5	$3p\ ^2P^0 - 3p'\ ^2P$						
						1616.3	9	$4d\ ^2D - 5f\ ^2F^0$
						1619.7	12	$4f\ ^2F^0 - 5g\ ^2G$
						1622.0	1	$4f\ ^2F^0 - 5d\ ^2D$
						1655.9	1	$4d\ ^2D - 5p\ ^2P^0$
						1656.0	1	$4d\ ^2D - 5p\ ^2P^0$
			1688.1	3	$4f\ ^3F^0 - 6g\ ^3G$			
			1696.9	3	$3d'\ ^3F^0 - 5g\ ^3G$			
			1699.0	4	$3d'\ ^3F^0 - 5g\ ^3G$			
1699.3	6	$3p'\ ^4D - 4s'\ ^4P^0$						
1700.0	5	$3p'\ ^4D - 4s'\ ^4P^0$						
			1702.0	5	$3d'\ ^3F^0 - 5g\ ^3G$			
						1702.2	3	$4p\ ^2P^0 - 5s\ ^2S$
						1703.2	4	$4p\ ^2P^0 - 5s\ ^2S$
			1718.5	20	$2p\ ^1P^0 - 2p^2\ ^1D$			
1727.4	5	$3d'\ ^4F^0 - 4f'\ ^2G$						
1729.9	10	$3d'\ ^4F^0 - 4f'\ ^4G$						
1746.8	0	$2p\ ^2P^0 - 2p^2\ ^2P$						
1747.8	15	$2p\ ^2P - 2p^3\ ^2D^0$						
1748.6	3	$2p\ ^2P^0 - 2p^2\ ^4P$						
1749.7	0	$2p\ ^2P^0 - 2p^2\ ^4P$						
1751.2	12	$2p^2\ ^2P - 2p^3\ ^2D^0$						
1751.7	16	$2p^2\ ^2P - 2p^3\ ^2D^0$						
1752.2	0	$2p\ ^2P^0 - 2p^2\ ^4P$						
1754.0	0	$2p\ ^2P^0 - 2p^2\ ^4P$						
1804.5	8	$3p\ ^2P^0 - 4s\ ^2S$						
1805.7	9	$3p\ ^2P^0 - 4s\ ^2S$						
						1811.6	1	$5p\ ^2P^0 - 7d\ ^2D$
						1857.7	3	$5d\ ^2D - 7f\ ^2F^0$
						1857.9	3	$5d\ ^2D - 7f\ ^2F^0$
						1860.4	6	$5fgh - 7ghi$
						1882.9	1	$5p\ ^2P^0 - 7s\ ^2S$
1885.0	12	$3d\ ^2D - 4f\ ^2F^0$						
1885.2	13	$3d\ ^2D - 4f\ ^2F^0$						
1949.3	6	$3p'\ ^4P - 4s'\ ^4P^0$						
			2035.6	5	$4p\ ^3P^0 - 5d\ ^3D$			
			2036.1	4	$4p\ ^3P^0 - 5d\ ^3D$			
			2080.3	6	$3d'\ ^1F^0 - 5g\ ^1G$			
2147.3	6	$3d'\ ^4F^0 - 4p'\ ^4D$						
2148.1	5	$3d'\ ^4F^0 - 4p'\ ^4D$						
2148.5	5	$3d'\ ^4F^0 - 4p'\ ^4D$						
2247.9	6	$3d\ ^2D - 4p\ ^2P^0$						
2248.9	5	$3d\ ^2D - 4p\ ^2P^0$						
			2318.1	6	$4d\ ^3D - 5f\ ^3F^0$			
			2402.0	5	$3s'\ ^1P^0 - 4d\ ^1D$			
			2421.6	3	$3d'\ ^3P^0 - 5d\ ^3D$			
			2430.4	3	$4p\ ^3P^0 - 5s\ ^3S$			
			2477.7	8	$4d\ ^1D - 5f\ ^1F^0$			
						2590.8	2	$5s\ ^2S - 6p\ ^2P^0$
						2591.4	1	$5s\ ^2S - 6p\ ^2P^0$
			2645.6	10	$4f\ ^3F^0 - 5g\ ^3G$			
			2646.2	11	$4f\ ^3F^0 - 5g\ ^3G$			
			2646.9	12	$4f\ ^3F^0 - 5g\ ^3G$			
2686.9	5	$4d\ ^2D - 6f\ ^2F^0$						
2689.2	6	$4d\ ^2D - 6f\ ^2F^0$						
						2858.0	4	$5p\ ^2P^0 - 6d\ ^2D$
						2859.2	5	$5p\ ^2P^0 - 6d\ ^2D$
2862.2	10	$4f\ ^2F^0 - 6g\ ^2G$						
			2884.8	4	$5g\ ^3G - 7h\ ^3H^0$			
2972.6	3	$3p'\ ^2P - 3d'\ ^2P^0$						
						2974.5	6	$5d\ ^2D - 6f\ ^2F^0$
						2980.8	8	$5f\ ^2F^0 - 6g\ ^2G$
						2981.3	10	$5g\ ^2G - 6h\ ^2H^0$
2983.6	4	$3p'\ ^2P - 3d'\ ^2P^0$						
						2998.4	5	$6fgh - 8ghi$
			3078.2	6	$4f\ ^1F^0 - 5g\ ^1G$			
			3141.2	3	$3p'\ ^3D - 4f\ ^3F^0$			
						3159.7	2	$5p\ ^2P^0 - 6s\ ^2S$

Table 5. continued

OIV			OV			OVI		
λ	I_{lab}	Transition	λ	I_{lab}	Transition	λ	I_{lab}	Transition
			1218.3	1	$2s\ ^1S - 2p\ ^3P^0$			
1338.6	11	$2p^2\ ^2P - 2p^3\ ^2D^0$						
1343.0	9	$2p^2\ ^2P - 2p^3\ ^2D^0$						
1343.5	12	$2p^2\ ^2P - 2p^3\ ^2D^0$						
			1371.3	20	$2p\ ^1P^0 - 2p^2\ ^1D$			
1397.2	3	$2p\ ^2P^0 - 2p^2\ ^4P$						
1399.8	5	$2p\ ^2P^0 - 2p^2\ ^4P$						
1401.2	7	$2p\ ^2P^0 - 2p^2\ ^4P$						
1404.8	4	$2p\ ^2P^0 - 2p^2\ ^4P$						
1407.4	5	$2p\ ^2P^0 - 2p^2\ ^4P$						
			1506.7	10	$4d\ ^3D - 5f\ ^3F^0$			
			1596.4	7	$4d\ ^1D - 5f\ ^1F^0$			
			1643.7	14	$4f\ ^3F^0 - 5g\ ^3G$			
			1708.0	10	$4f\ ^1F^0 - 5g\ ^1G$			
						2069.9	3	$5f\ ^2F^0 - 6g\ ^2G$
						2070.3	4	$5f\ ^2G^0 - 6h\ ^2H$
						2081.8	2	$6f\ ^2F - 8g\ ^2G$
						2082.3	2	$6g\ ^2G - 8h\ ^2H^0$
2384.6	7	$4d\ ^2D - 5f\ ^2F^0$						
2449.4	11	$4f\ ^2F^0 - 5g\ ^2G$						
2450.0	11	$4f\ ^2F^0 - 5g\ ^2G$						
						2482.0		$7g\ ^2G - 10h\ ^2H^0$
2493.4	11	$3s'\ ^4P^0 - 3p'\ ^4P$						
2493.8	11	$3s'\ ^4P^0 - 3p'\ ^4P$						
2499.3	7	$3s'\ ^4P^0 - 3p'\ ^4P$						
2501.8	7	$3s'\ ^4P^0 - 3p'\ ^4P$						
2507.7	11	$3s'\ ^4P^0 - 3d'\ ^4P$						
2509.2	12	$3s'\ ^4P^0 - 3p'\ ^4P$						
2517.4	11	$3s'\ ^4P^0 - 3p'\ ^4P$						
			2695.4	6	$5f\ ^3F^0 - 4f'\ ^3G$			
			2755.1	8	$3s'\ ^3P^0 - 3p'\ ^3P$			
2758.2	7	$4d\ ^2D - 5p\ ^2P^0$						
			2781.0	25	$3s\ ^3S - 3p\ ^3P^0$			
			2787.0	24	$3s\ ^3S - 3p\ ^3P^0$			
			2789.8	22	$3s\ ^3S - 3p\ ^3P^0$			
2805.8	8	$3s'\ ^4P^0 - 3p'\ ^4S$						
2816.6	9	$3s'\ ^4P^0 - 3p'\ ^4S$						
2836.3	10	$3s'\ ^4P^0 - 3p'\ ^4S$						
2916.3	9	$3p'\ ^2P - 3d'\ ^2D^0$						
2921.5	10	$3p'\ ^4P - 3d'\ ^2D^0$						
			2941.3	11	$5g\ ^3G - 6h\ ^3H^0$			
			2941.6	11	$5g\ ^{3,1}G - 6h\ ^{3,1}H^0$			
3028.0	7	$3s'\ ^2P^0 - 4s'\ ^2S$						
3052.5	8	$3s'\ ^2P^0 - 4s'\ ^2S$						
3063.4	17	$3s\ ^2S - 3p\ ^2P^0$						
						3071.3		$6s\ ^2S - 7p\ ^2P^0$
3071.6	16	$3s\ ^2S - 3p\ ^2P^0$						
						3142		$7g\ ^2G - 9h\ ^2H^0$
			3144.7	10	$3p\ ^1P^0 - 3d\ ^1D$			
			3156.1	7	$5f\ ^3F^0 - 6g\ ^3G$			
			3168.1	6	$5f\ ^3F^0 - 6g\ ^3G$			
			3172.3	5	$5f\ ^3F^0 - 6g\ ^3G$			
			3176.9	6	$5f\ ^1F^0 - 6g\ ^1G$			
3180.9	8	$3p'\ ^4D - 3d'\ ^4D^0$						
3185.9	7	$3p'\ ^4D - 3d'\ ^4D^0$						
3194.8	9	$3p'\ ^4D - 3d'\ ^4D^0$						
3199.6	7	$3p'\ ^4D - 3d'\ ^4D^0$						
3209.7	10	$3p'\ ^4D - 3d'\ ^4D^0$						

Table 5. continued

CII			CIII			CIV		
λ	I_{lab}	Transition	λ	I_{lab}	Transition	λ	I_{lab}	Transition
			1175.7	5	$2p\ ^3P^0 - 2p^2\ ^3P$			
			1176.0	3	$2p\ ^3P^0 - 2p^2\ ^3P$			
			1176.4	3	$2p\ ^3P^0 - 2p^2\ ^3P$			
						1230.5	3	$3p\ ^2P^0 - 4s\ ^2S$
			1247.4	3	$2p\ ^1P^0 - 2p^2\ ^1S$			
1323.9	9	$2p^2\ ^2D - 2p^3\ ^2D^0$						
1334.5	13	$2p\ ^2P^0 - 2p^2\ ^2D$						
1335.7	14	$2p\ ^2P^0 - 2p^2\ ^2D$						
			1426.4	4	$3s\ ^3S - 3s'\ ^3P^0$			
			1427.8	3	$3s\ ^3S - 3s'\ ^3P^0$			
			1477.7	3	$3d\ ^3D - 3d'\ ^3D^0$			
						1548.2	20	$2s\ ^2S - 2p\ ^2P^0$
						1550.8	19	$2s\ ^2S - 2p\ ^2P^0$
			1576.5	3	$3d\ ^3D - 3d'\ ^3F^0$			
			1620.0	3	$3p\ ^3P^0 - 4d\ ^3D$			
			1908.7		$2s^2\ ^1S - 2p\ ^3P^0$			
			1922.9	5	$3d\ ^3D - 4f\ ^3F^0$			
			1923.1	4	$3d\ ^3D - 4f\ ^3F^0$			
			2009.6	4	$3p\ ^3P^0 - 4s\ ^3S$			
			2010.1	5	$3p\ ^3P^0 - 4s\ ^3S$			
			2092.0	6	$3d\ ^3D - 4p\ ^3P^0$			
			2162.9	9	$3d\ ^1D - 4f\ ^1F^0$			
			2177.0	4	$3d\ ^1D - 4p\ ^1P^0$			
			2296.9	16	$2p\ ^1P^0 - 2p^2\ ^1D$			
2323.5	0	$2p^3\ ^4S^0 - 3p'\ ^4S$						
2324.7	0	$2p\ ^2P^0 - 2p^2\ ^4P$						
2325.4	0	$2p\ ^2P^0 - 2p^2\ ^4P$						
2326.9	0	$2p\ ^2P^0 - 2p^2\ ^4P$						
2328.1	0	$2p\ ^2P^0 - 2p^2\ ^4P$						
						2335.9	2	$5g^2G - 8h^2H^0$
2401.8	5	$2p\ ^2P^0 - 5s\ ^2S$						
2402.4	7	$3p\ ^2P^0 - 5s\ ^2S$						
						2404.4	5	$4p\ ^2P^0 - 5d\ ^2D$
						2405.1	6	$4p\ ^2P^0 - 5d\ ^2D$
						2423.7	4	$4d\ ^2D - 5g\ ^2G$
			2480.5	4	$4p\ ^3P^0 - 6d\ ^3D$			
			2480.9	4	$4p\ ^3P^0 - 6d\ ^3D$			
2509.1	10	$2p^2\ ^2P - 2p^3\ ^2D^0$						
2512.1	12	$2p^2\ ^2P - 2p^3\ ^2D^0$						
						2524.4	9	$4d\ ^2D - 5f\ ^2F^0$
						2530.0	11	$4f\ ^2F^0 - 5g\ ^2G$
						2530.6	6	$4f\ ^2F^0 - 5f\ ^2F^0$
2574.8	10	$3d\ ^2D - 6f\ ^2F$						
						2595.1	4	$4d\ ^2D - 5p\ ^2P^0$
						2595.3	3	$4d\ ^2D - 5p\ ^2P^0$
			2610.0	6	$3d\ ^3D - 3s'\ ^3P^0$			
			2614.5	5	$3d\ ^3D - 3s'\ ^3P^0$			
			2616.6	4	$3d\ ^3D - 3s'\ ^3P^0$			
2640.6	6	$3p'\ ^4D - 4d'\ ^4F^0$						
2640.9	5	$3p'\ ^4D - 4d'\ ^4F^0$						
2641.4	8	$3p'\ ^4D - 4d'\ ^4F^0$						
			2670.2	3	$4d\ ^3D - 6f\ ^3F^0$			
			2671.3	4	$4d\ ^3D - 6f\ ^3F^0$			
			2673.0	5	$4d\ ^3D - 6f\ ^3F^0$			
			2697.4	3	$4p\ ^3P^0 - 6s\ ^3S$			
						2697.7	4	$4p\ ^2P^0 - 5s\ ^2S$
			2697.7	7	$4p\ ^3P^0 - 6s\ ^3S$			
						2698.7	4	$4p\ ^2P^0 - 5s\ ^2S$
			2724.8	6	$4f\ ^3F^0 - 6g\ ^3G$			
			2725.3	7	$4f\ ^3F^0 - 6g\ ^3G$			
			2725.9	7	$4f\ ^3F^0 - 6g\ ^3G$			
2746.5	10	$3p\ ^2P^0 - 4d\ ^2D$						
2747.3	12	$3p\ ^2P^0 - 4d\ ^2D$						
			2751.8	3	$4p\ ^1P^0 - 6d\ ^1D$			
			2777.7	5	$4f\ ^1F^0 - 6g\ ^1G$			
			2796.5	3	$4f\ ^1F^0 - 6g\ ^1G$			
			2799.5	4	$4f\ ^1F^0 - 6g\ ^1G$			
2801.2	5	$3d'\ ^4F^0 - 5f'\ ^4G$						
2801.4	5	$3d'\ ^4F^0 - 5f'\ ^4G$						
2836.7	20	$2p^2\ ^2S - 3p\ ^2P^0$						
2837.6	18	$2p^2\ ^2S - 3p\ ^2P^0$						
			2849.0	5	$3s'\ ^1P^0 - 3p'\ ^1S$			
			2863.7	4	$4d\ ^1D - 6f\ ^1F^0$			
			2874.7	3	$4s\ ^3S - 5p\ ^3P^0$			
2885.5	6	$3d'\ ^4D^0 - 5f'\ ^2F$						
						2906.3	5	$5g\ ^2G - 7h\ ^2H^0$
2966.9	5	$3p'\ ^4P - 4d'\ ^4D^0$						
2967.9	7	$3p'\ ^4P - 4d'\ ^4D^0$						
			2982.1	8	$3d\ ^1D - 3s'\ ^1P^0$			
2992.6	18	$3d\ ^2D - 5f\ ^2F^0$						
3165.5	9	$2p^3\ ^2D^0 - 3p'\ ^2P$						
3167.9	8	$2p^3\ ^2D^0 - 3p'\ ^2P$						
			3170.0	4	$4s\ ^1S - 5p\ ^1P^0$			

Table 5. continued

OIII			SiIII			SiIV		
λ	I_{lab}	Transition	λ	I_{lab}	Transition	λ	I_{lab}	Transition
						1128.3	10	$3p\ ^2P^0 - 3d\ ^2D$
			1206.5	30	$3s^2\ ^1S - 3p\ ^1P^0$			
			1206.5	30	$3p\ ^1P^0 - 3d\ ^1D$			
			1207.5	9	$3p^2\ ^1D - 3d'\ ^1D^0$			
			1210.5	10	$3p^2\ ^1D - 4f\ ^1F^0$			
			1294.5	17	$3p\ ^3P^0 - 3p^2\ ^3P$			
			1296.7	14	$3p\ ^3P^0 - 3p^2\ ^3P$			
			1298.9	15	$3p\ ^3P^0 - 3p^2\ ^3P$			
			1299.0	18	$3p\ ^3P^0 - 3p^2\ ^3P$			
			1301.1	14	$3p\ ^3P^0 - 3p^2\ ^3P$			
			1303.3	16	$3p\ ^3P^0 - 3p^2\ ^3P$			
			1312.6	13	$3p\ ^1P^0 - 4s\ ^1S$			
						1393.8	15	$3s\ ^2S - 3p\ ^2P^0$
						1402.8	12	$3s\ ^2S - 3p\ ^2P^0$
			1417.2	13	$3p\ ^1P^0 - 3p^2\ ^1S$			
			1500.2	12	$3d\ ^3D - 4f\ ^3F^0$			
			1501.2	10	$3d\ ^3D - 4f\ ^3F^0$			
			1501.9	9	$3d\ ^3D - 4f\ ^3F^0$			
1590.0	8	$3p\ ^3D - 4s\ ^3P^0$						
						1722.5	6	$3d\ ^2D - 4p\ ^2P^0$
						1727.4	5	$3d\ ^2D - 4p\ ^2P^0$
1760.1	7	$3d\ ^3F^0 - 4f\ G[9/2]$						
1763.2	7	$3d\ ^3F^0 - 4f\ G[7/2]$						
1764.5	7	$3d\ ^3F^0 - 4s\ ^3P^0$						
1767.8	13	$3d\ ^3F^0 - 4f\ G[9/2]$						
1768.2	11	$3d\ ^3F^0 - 4f\ G[7/2]$						
1771.7	9	$3d\ ^1D^0 - 4f\ G[7/2]$						
1779.2	7	$3d\ ^3F^0 - 4f\ F[7/2]$						
1789.7	7	$3d\ ^1D^0 - 4f\ F[5/2]$						
			1842.6	9	$3p^2\ ^1D - 4p\ ^1P^0$			
1872.8	8	$3d\ ^3D^0 - 4f\ F[7/2]$						
1872.9	8	$3d\ ^3D^0 - 4f\ F[5/2]$						
1874.9	8	$3d\ ^3F^0 - 4f\ F[5/2]$						
1923.5	7	$3d\ ^3P0 - 4f\ D[5/2]$						
2013.3	9	$3d\ ^1F^0 - 4f\ G[9/2]$						
2045.7	7	$3d\ ^1P^0 - 4f\ D[3/2]$						
						2287.0	5	$4d\ ^2D - 5f\ ^2F^0$
			2296.9	10	$3d'\ ^1F^0 - 4f'\ /7/2/$			
			2308.2	10	$3d'\ ^3F^0 - 6g\ ^3G$			
2382.3	7	$3d\ ^3F^0 - 4p\ ^3D$						
2390.4	8	$3d\ ^1P^0 - 3p\ ^1P^0$						
			2449.5	11	$4d\ ^3D - 6f\ ^3F^0$			
2455.0	8	$3s\ ^1P^0 - 3p\ ^1S$						
						2517.5	7	$4f\ ^2F^0 - 5g\ ^2G$
			2541.8	25	$3p\ ^1P^0 - 3p^2\ ^1D$			
			2546.1	10	$3d\ ^1D - 3d'\ ^1D^0$			
2558.1	8	$3d\ ^1F^0 - 4p\ ^1D$						
			2559.2	14	$3d\ ^1D - 4f\ ^1F^0$			
2597.7	8	$3d\ ^3P^0 - 4p\ ^3S$						
			2640.8	11	$3d'\ ^1D^0 - 4p'\ ^1P$			
			2655.5	14	$4f\ ^1F^0 - 6g\ ^1G$			
2665.7	7	$3s'\ ^5P - 3p'\ ^5S^0$						
2674.6	8	$3s'\ ^5P - 3p'\ ^5S^0$						
2686.1	10	$3s'\ ^5P - 3p'\ ^5S^0$						
			2817.1	9	$4f\ ^3F^0 - 4p'\ ^3D$			
2983.8	9	$3s\ ^1P^0 - 3p\ ^1D$						
			3040.9	9	$4f\ ^3F^0 - 6g\ ^3G$			
3047.1	8	$3s\ ^3P^0 - 3p\ ^3P$						
			3086.2	25	$3d\ ^3D - 4p\ ^3P^0$			
			3093.4	20	$3d\ ^3D - 4p\ ^3P^0$			
			3096.8	16	$3d\ ^3D - 4p\ ^3P^0$			
						3149.6	7	$4p\ ^2P^0 - 4d\ ^2D$
						3165.7	9	$4p\ ^2P^0 - 4d\ ^2D$
			3185.1	16	$4p\ ^1P^0 - 5s\ ^1S$			
			3186.0	13	$3d'\ ^3F^0 - 5g\ ^3G$			
			3196.5	14	$3d'\ ^3F^0 - 5g\ ^3G$			
			3210.5	15	$3d'\ ^3F^0 - 5g\ ^3G$			

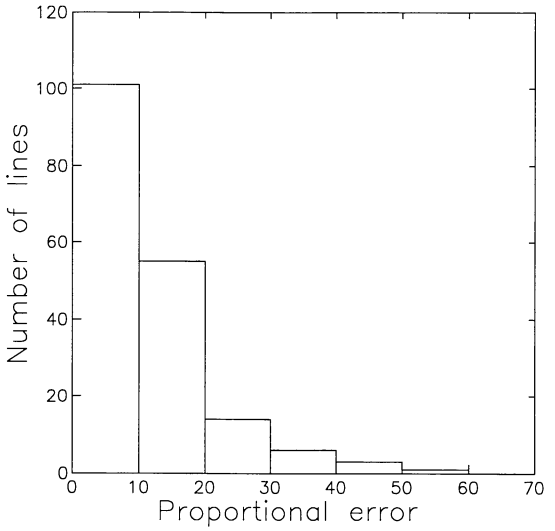

Fig. 1. Proportional error [in %] distribution histogram

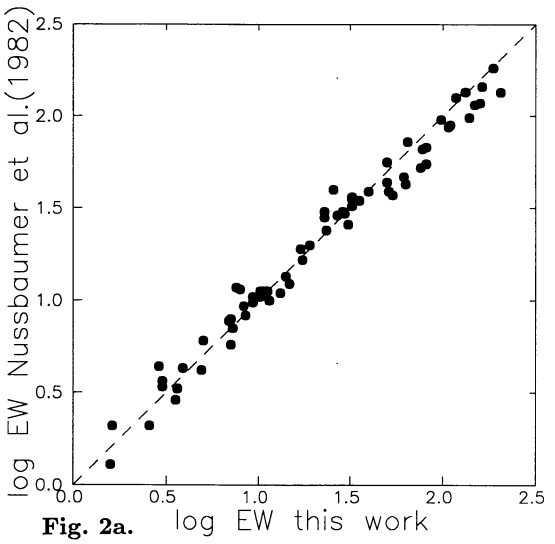

Fig. 2a.

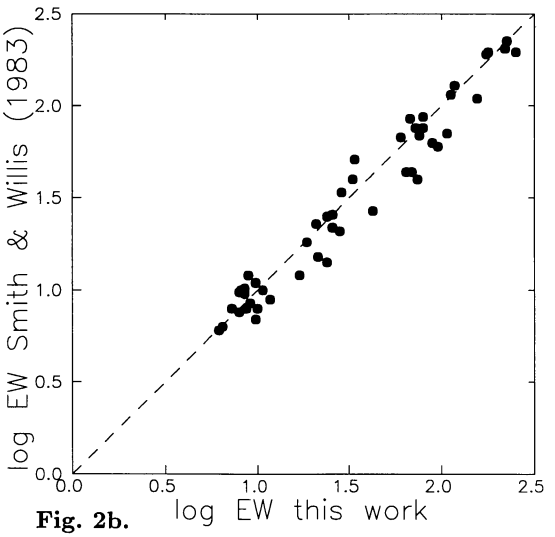

Fig. 2b.

Fig. 2. A comparison of our and literature data for stars in common with: a) Nussbaumer et al. (1982), b) Smith & Willis (1983)

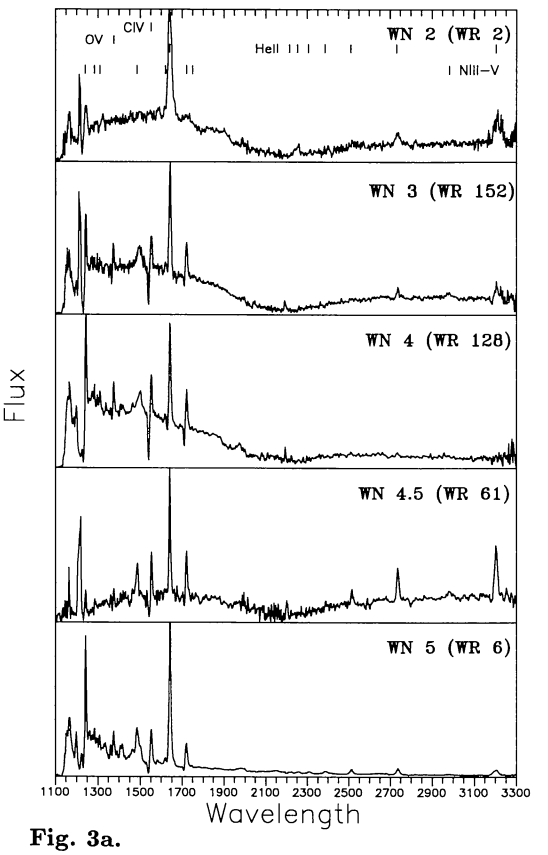

Fig. 3a.

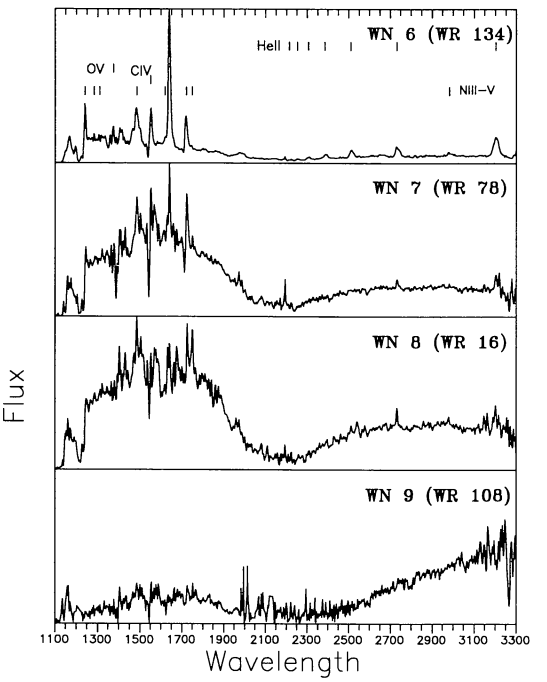

Fig. 3b.

Fig. 3. Representative tracings of low resolution IUE spectra of WR stars of different spectral types: a) WN 2 – 5 stars, b) WN 6 – 9 stars

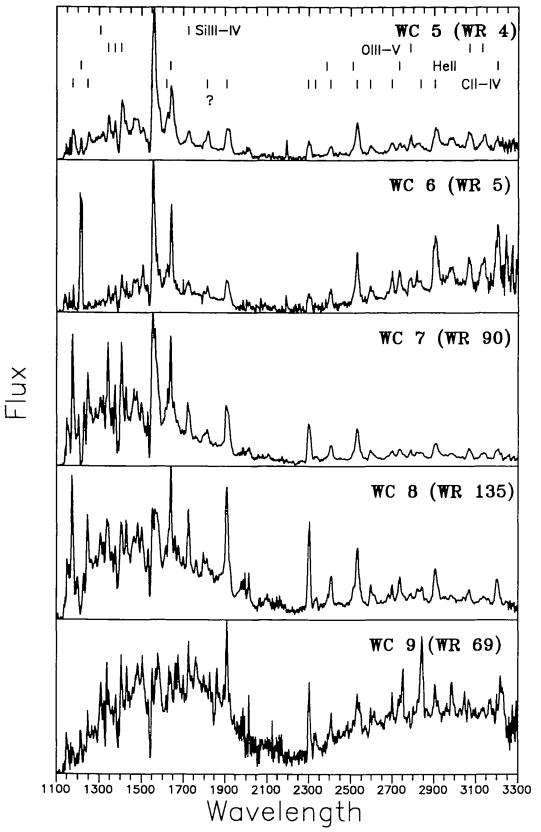

Fig. 4. Representative tracings of low resolution IUE spectra of WC 5 – 9 stars

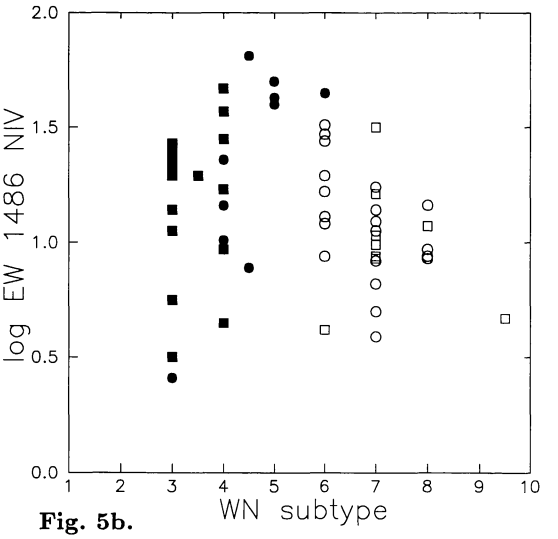

Fig. 5b.

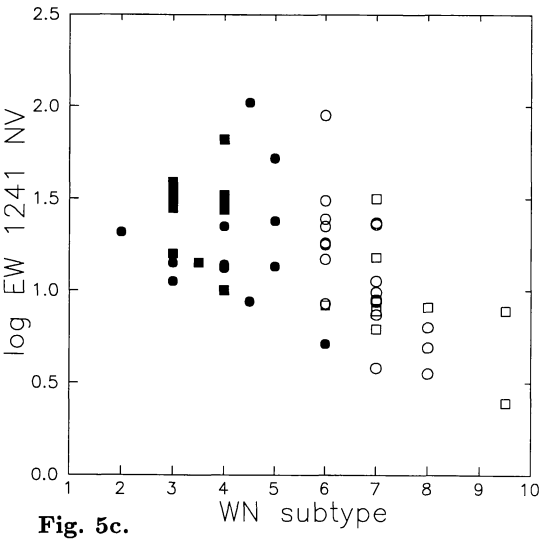

Fig. 5c.

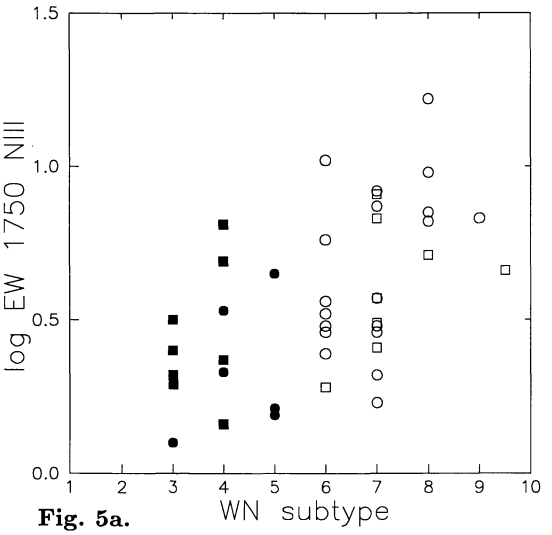

Fig. 5a.

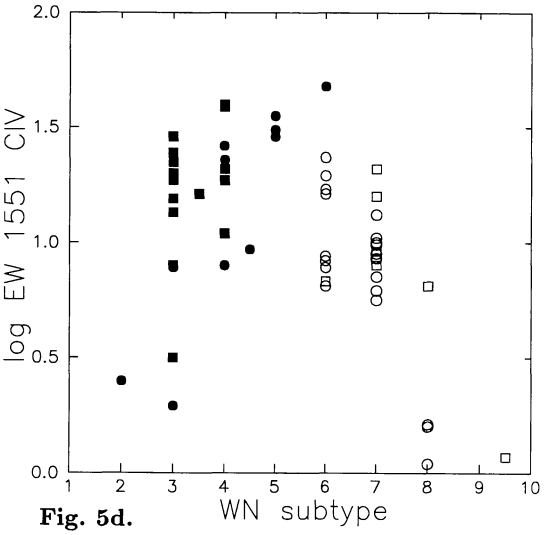

Fig. 5d.

Fig. 5. A correlation with spectral type of equivalent widths (Log EW [Å]) of different UV emission lines of nitrogen and carbon and silicon in WN stars (see text for discussion): a) nitrogen NIII 1750, b) nitrogen NIV 1486, c) nitrogen NV 1241, d) carbon CIV 1551, e) silicon SiIV 1406. (In Figs. 5-15 the different symbols denote: dark circles - Galactic WNE or WCE, open circles - Galactic WNL or WCL, dark squares - LMC WNE or WCE, open squares - LMS WNL or WCL)

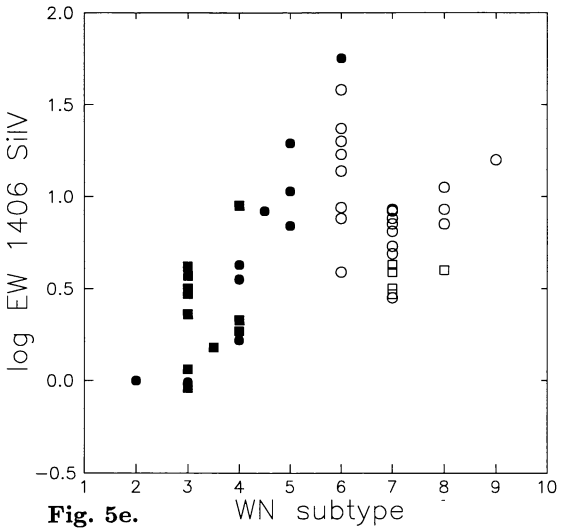

Fig. 5e.

Fig. 5. continued

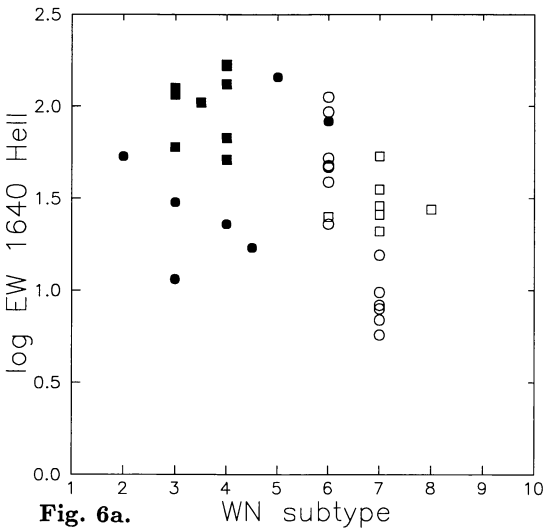

Fig. 6a.

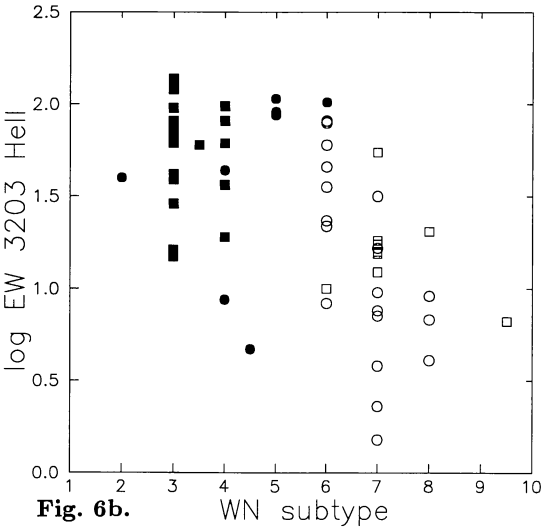

Fig. 6b.

Fig. 6. A correlation with spectral type of equivalent widths (Log EW [Å]) of different UV emission lines of helium in WN stars (see text for discussion): a) HeII 1640 (3-2), b) HeII 3203 (5-3)

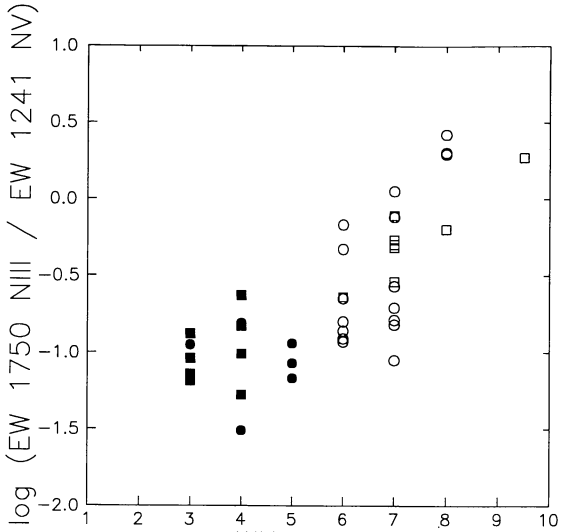

Fig. 7a.

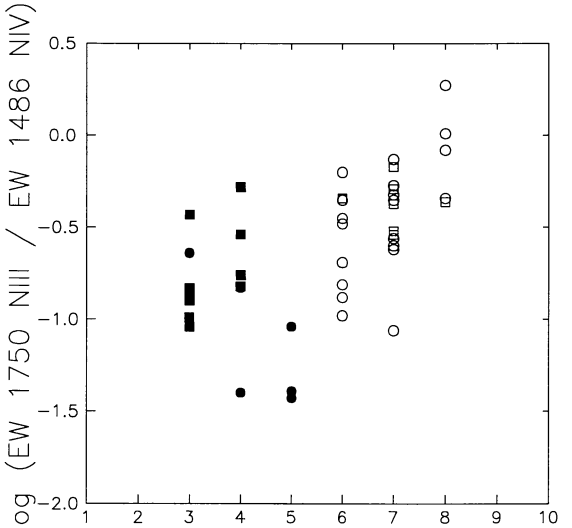

Fig. 7b.

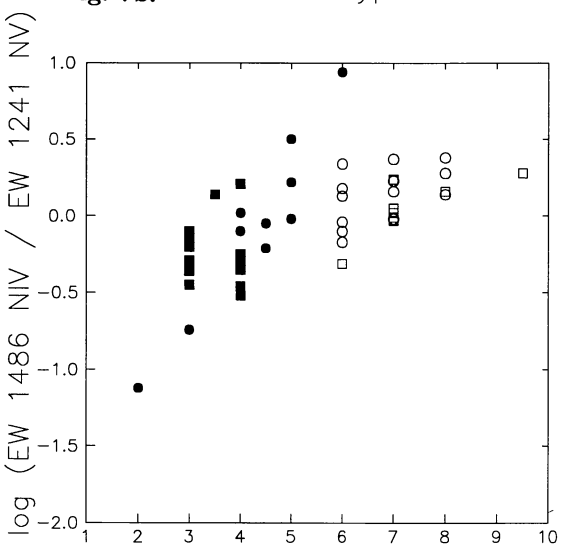

Fig. 7c.

Fig. 7. A correlation with spectral type of equivalent widths ratio (Log EW [Å]) of different UV emission lines of nitrogen in WN stars (see text for discussion): a) NIII 1750 to NV 1241 ratio, b) NIII 1750 to NIV 1486 ratio, c) NIV 1486 to NV 1241 ratio

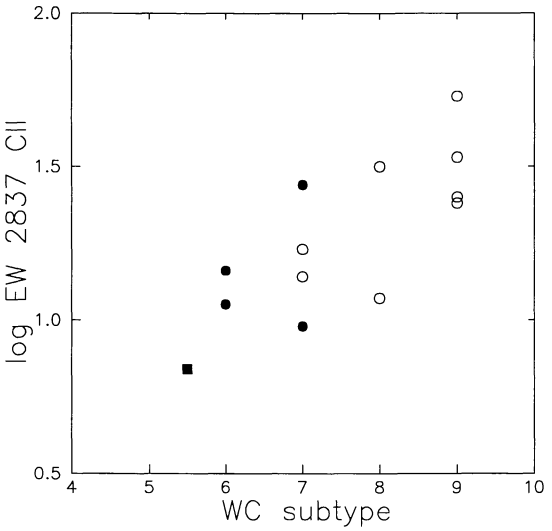

Fig. 8a.

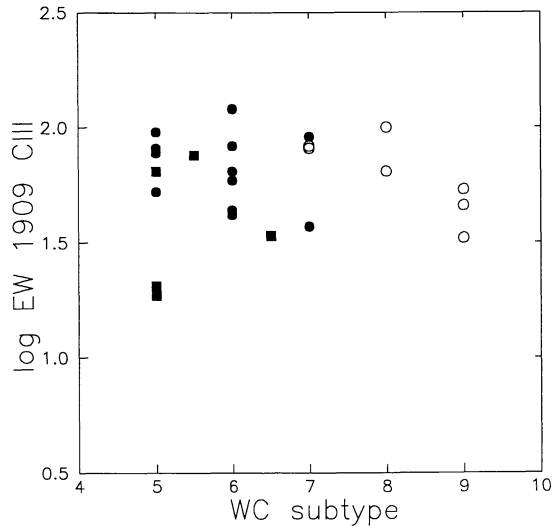

Fig. 8b.

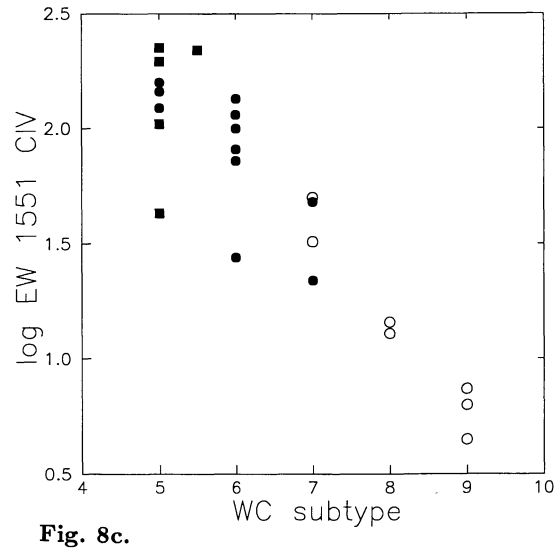

Fig. 8c.

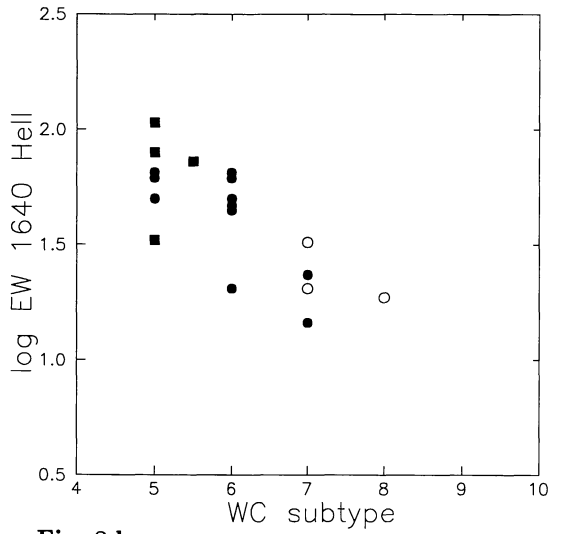

Fig. 8d.

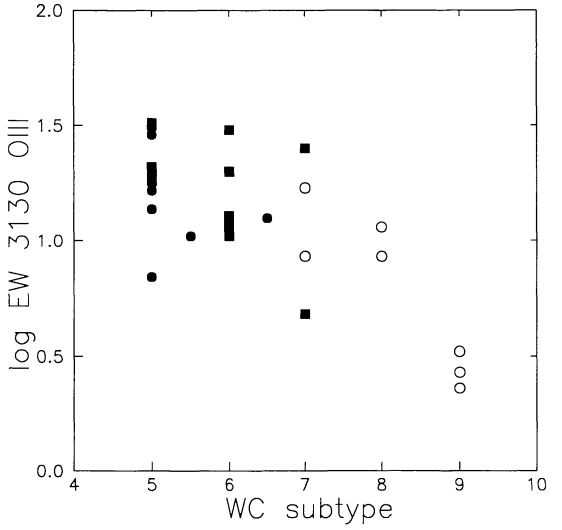

Fig. 8e.

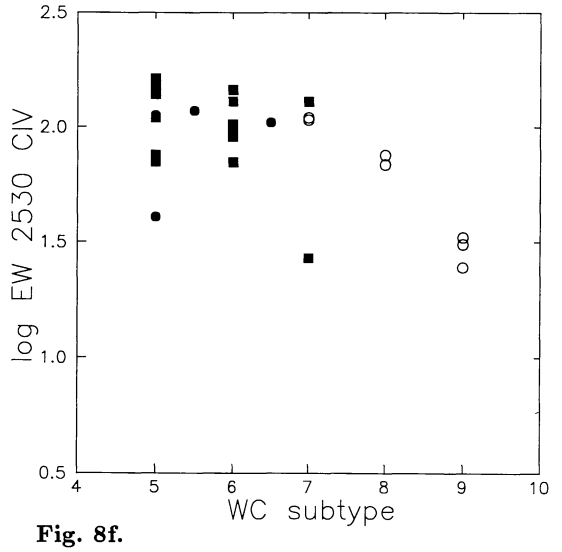

Fig. 8f.

Fig. 8. A correlation with spectral type of equivalent widths (Log EW [Å]) of different UV emission lines of carbon, helium and oxygen in WC stars (see text for discussion): a) carbon CII 2837, b) carbon CIII 1909, c) carbon CIV 1551, d) helium HeII 1640, e) oxygen OIII 3130 f) carbon CIV 2530

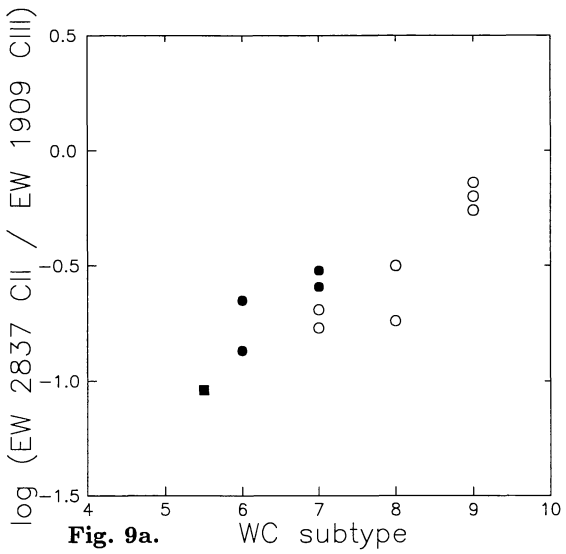

Fig. 9a.

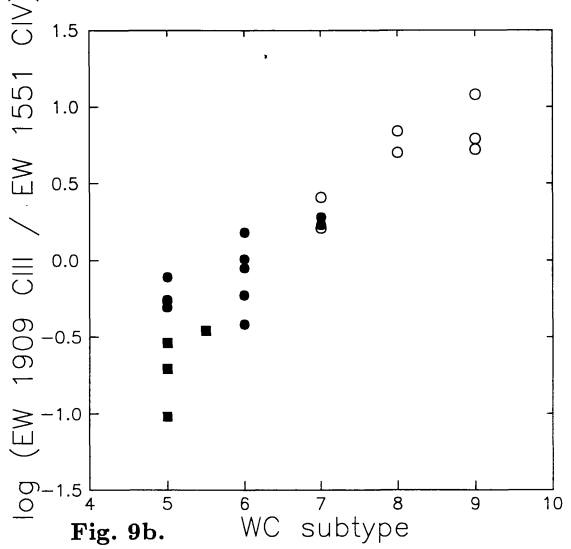

Fig. 9b.

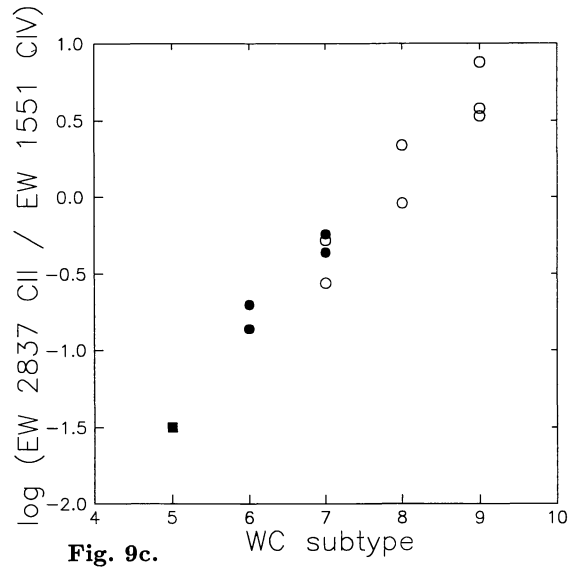

Fig. 9c.

Fig. 9. A correlation with spectral type of equivalent widths ratio (Log EW [Å]) of different UV emission lines of carbon in WC stars (see text for discussion): a) CII 2837 to CIII 1909 ratio, b) CIII 1909 to CIV 1551 ratio, c) CII 2837 to CIV 1551 ratio

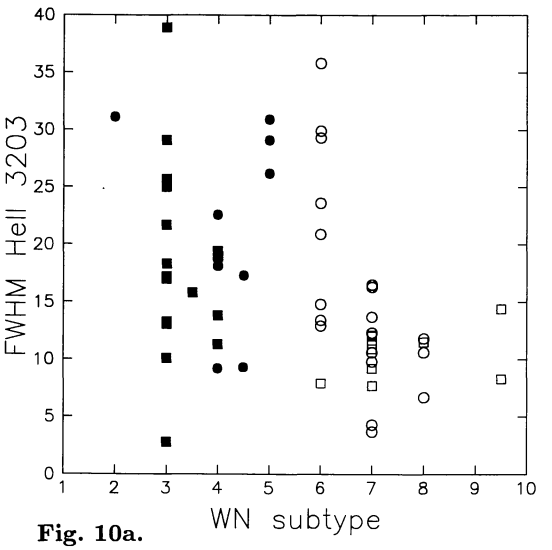

Fig. 10a.

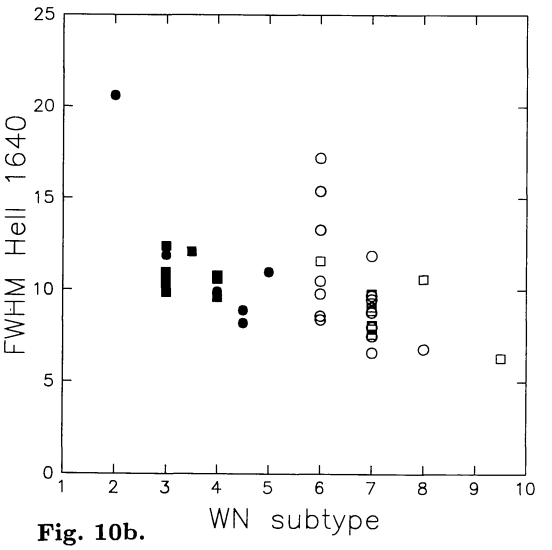

Fig. 10b.

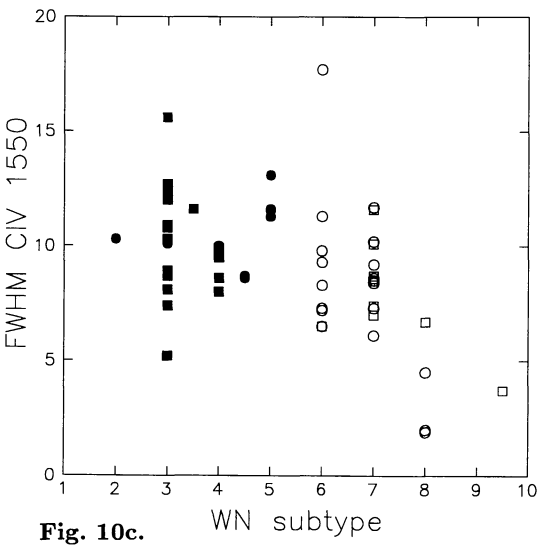

Fig. 10c.

Fig. 10. A correlation with spectral type of line widths (FWHM in Å) of the strongest emission lines in WN stars: a) helium HeII 3203, b) helium HeII 1640, c) carbon CIV 1551, d) nitrogen NIV 1486

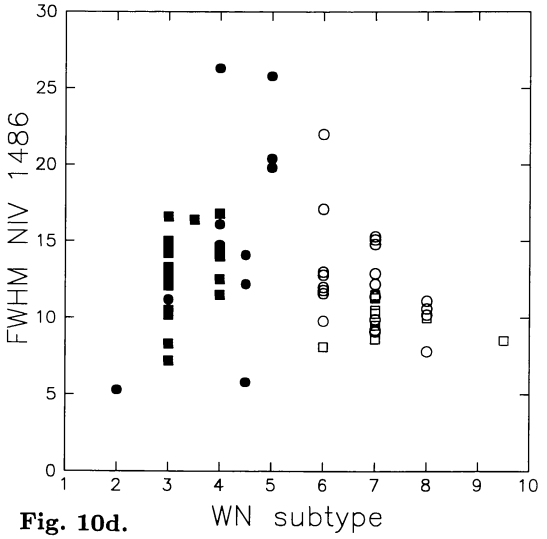

Fig. 10d.

Fig. 10. continued

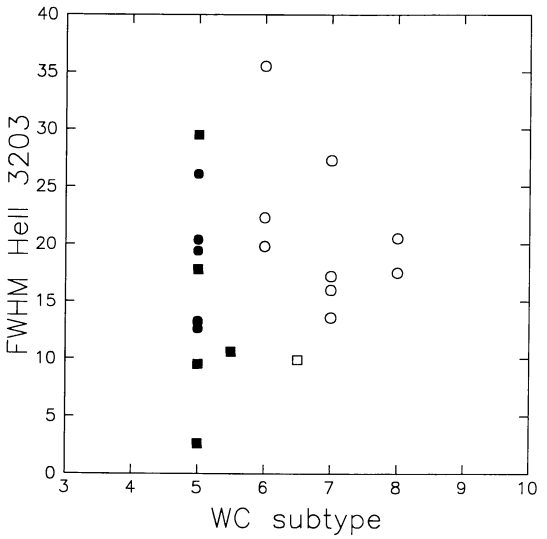

Fig. 11a.

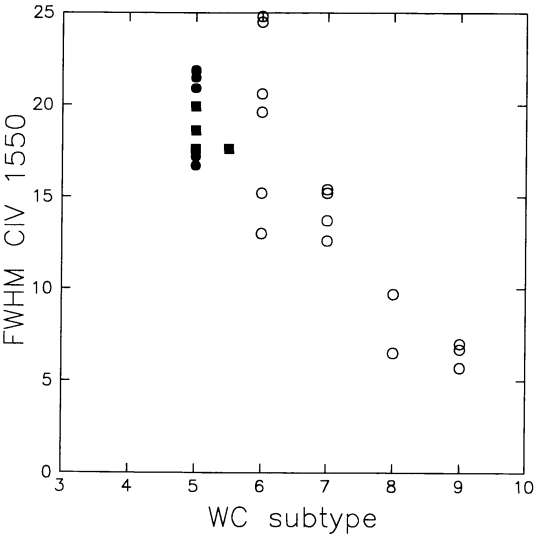

Fig. 11b.

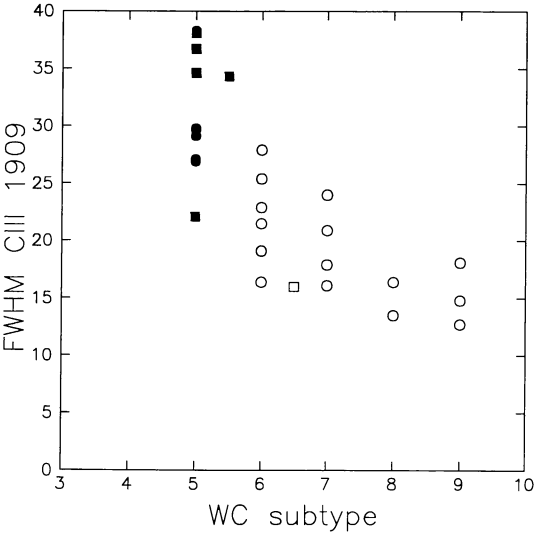

Fig. 11c.

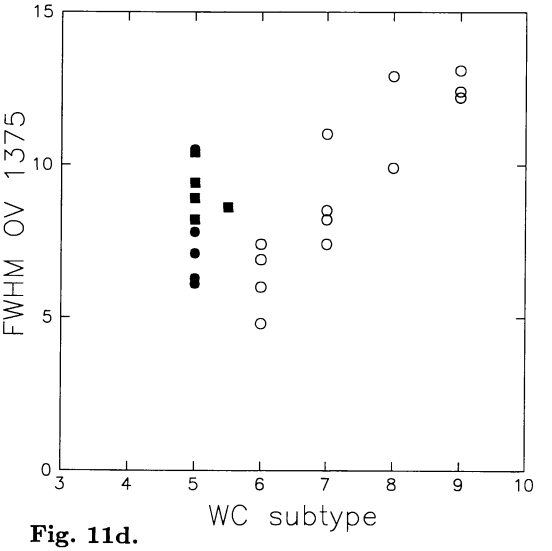

Fig. 11d.

Fig. 11. A correlation with spectral type of line widths (FWHM in Å) of the strongest emission lines in WC stars: a) helium HeII 3203, b) carbon CIV 1551, c) carbon CIII 1909, d) oxygen OV 1375

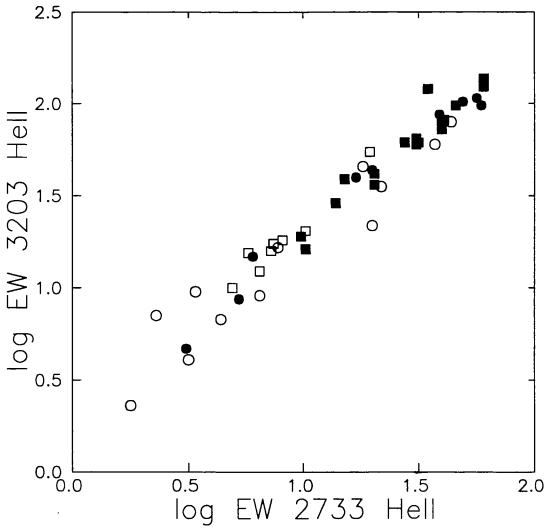

Fig. 12a.

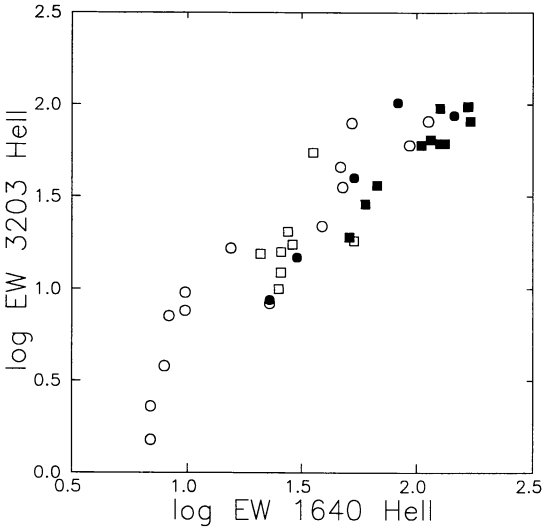

Fig. 12c.

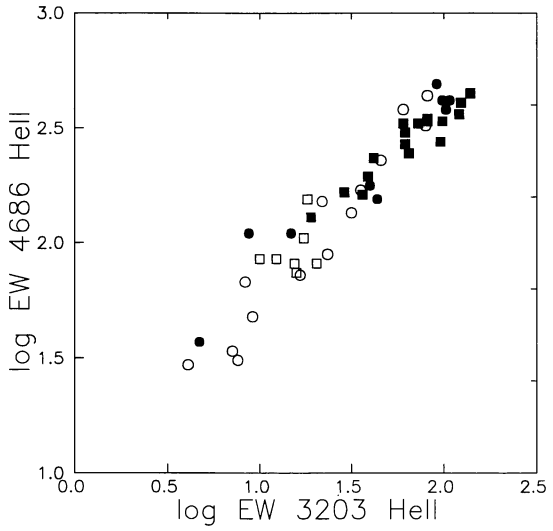

Fig. 12b.

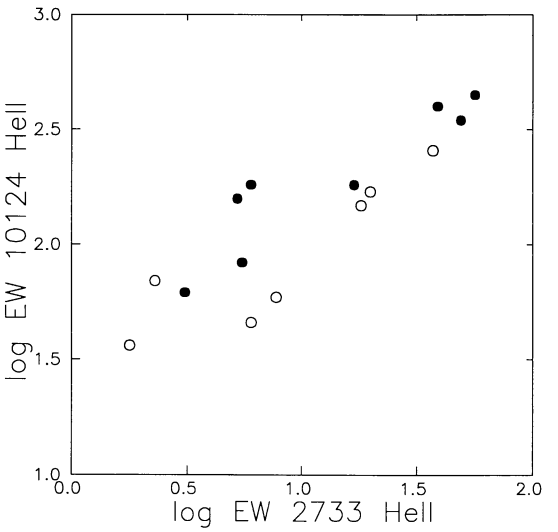

Fig. 12d.

Fig. 12. A correlation between equivalent widths (Log EW [Å]) of different helium lines in WN stars (see text for discussion): a) 3202 (5-3) vs. 2733 (6-3), b) 4686 (4-3) vs. 3203 (5-3), c) 3203 (5-3) vs. 1640 (3-2), d) 10124 (5-4) vs. 2733 (6-3)

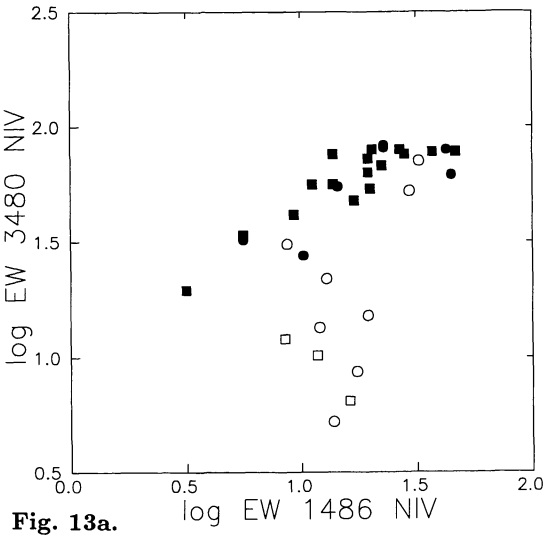

Fig. 13a.

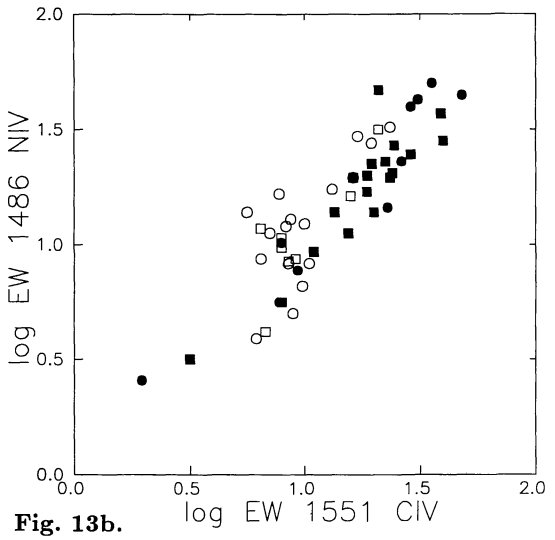

Fig. 13b.

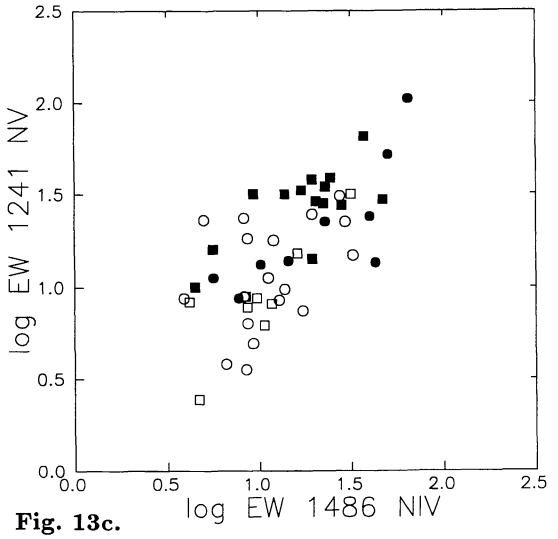

Fig. 13c.

Fig. 13. A correlation between equivalent widths (Log EW [Å]) of different nitrogen and carbon lines in WN stars (see text for discussion): a) nitrogen NIV 3480 vs. NIV 1486, b) nitrogen NIV 1486 vs. carbon CIV 1551, c) nitrogen NV 1241 vs. nitrogen NIV 1486

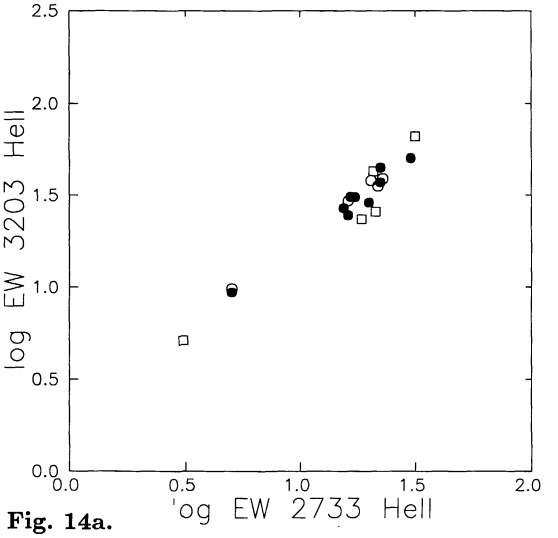

Fig. 14a.

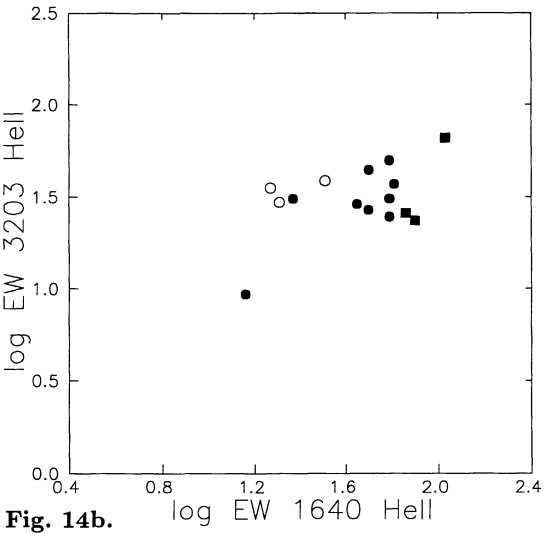

Fig. 14b.

Fig. 14. A correlation between equivalent widths (Log EW [Å]) of different helium lines in WC stars (see text for discussion): a) 3203 (5-3) vs. 2733 (6-3), b) 3202 (5-3) vs. 1640 (3-2)

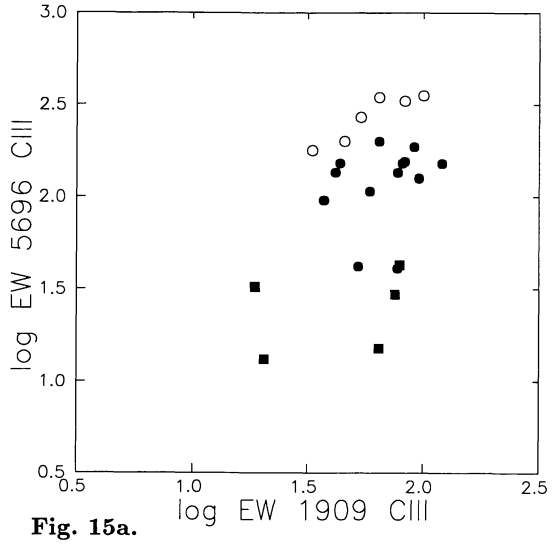

Fig. 15a.

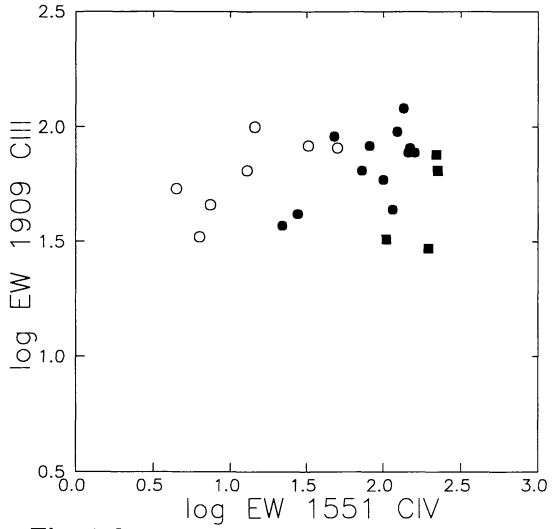

Fig. 15b.

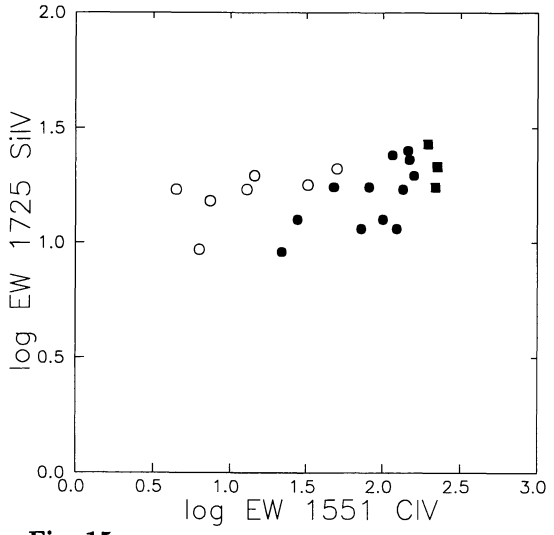

Fig. 15c.

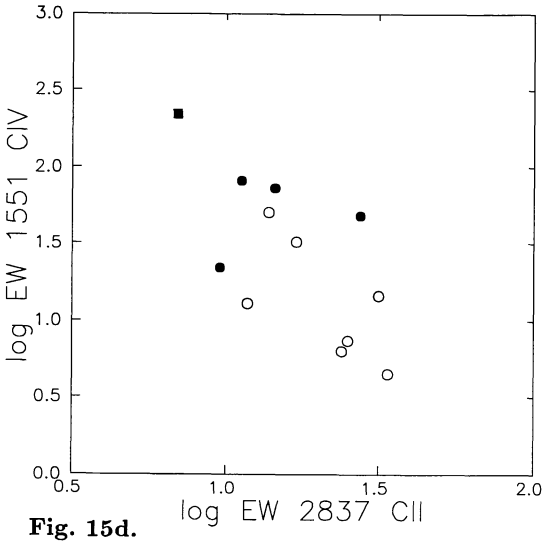

Fig. 15d.

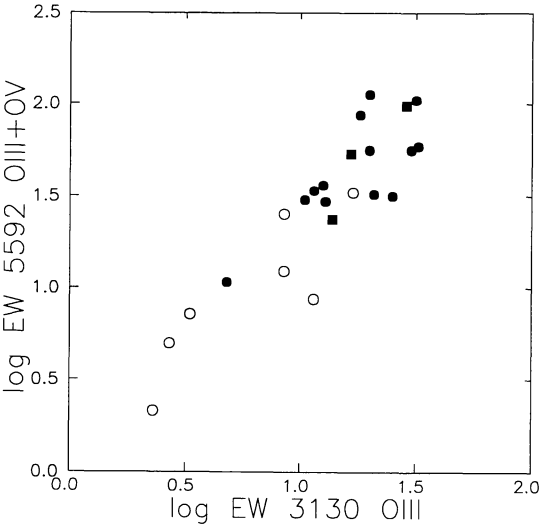

Fig. 15e.

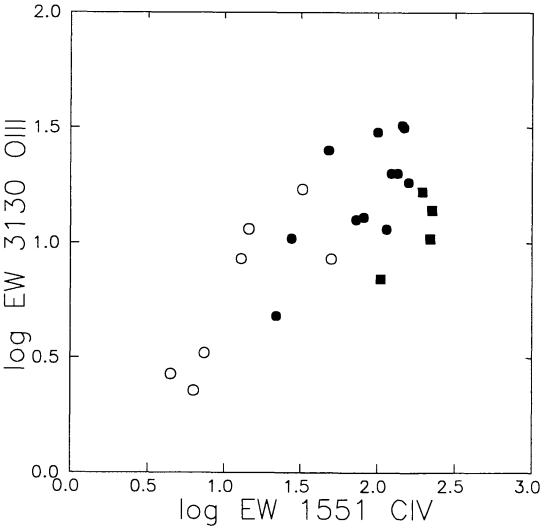

Fig. 15f.

Fig. 15. A correlation between equivalent widths (Log EW [Å]) of different emission lines in WC stars (see text for discussion): a) CIII 5696 vs. CIII 1909, b) CIII 1909 vs. CIV 1551, c) SiIV 1725 vs. CIV 1551, d) CIV 1551 vs. CII 2837, e) OIII-V blend 5592 vs. OIII 3130, f) OIII 3130 vs. CIV 1551

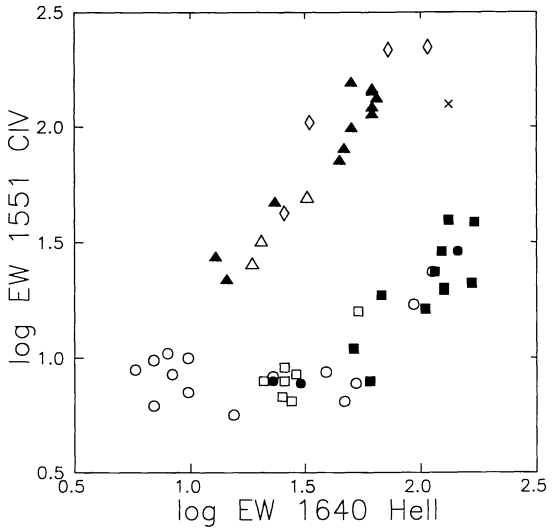

Fig. 16a.

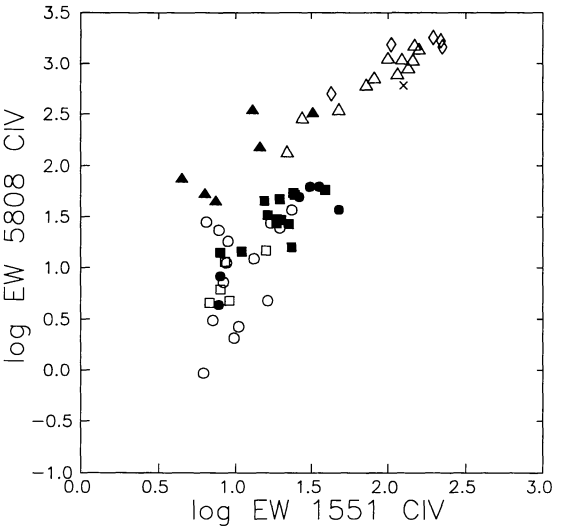

Fig. 16b.

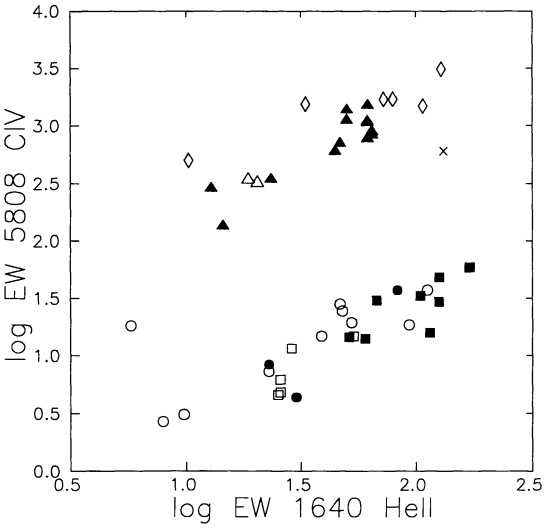

Fig. 16c.

Fig. 16. A correlation between equivalent widths (Log EW [Å]) of carbon and helium lines for WN and WC stars together (see text for discussion): a) CIV 1551 vs. HeII 1640, b) CIV 5808 vs. CIV 1551, c) CIV 5808 vs. HeII 1640. (Here the symbols have the following meaning: dark circles - Galactic WNE, open circles - Galactic WNL, dark squares - LMC WNE, open squares - LMC WNL, dark triangles - Galactic WCE, open triangles - Galactic WCL, open diamond - LMC WCL, cross - the only WN/WC star in our sample - Br29)